LIMNOLOGY and OCEANOGRAPHY

ASLO

Limnol. Oceanogr. 65, 2020, 1573–1593

doi: 10.1002/lno.11407

Modeling the coupled dynamics of stream metabolism and microbial biomass

Pier Luigi Segatto,[1] **Tom J. Battin**,[1] **Enrico Bertuzzo**[2*]

[1]Stream Biofilm and Ecosystem Research Laboratory, Ecole Polytechinque Fédérale de Lausanne, Lausanne, Switzerland
[2]Department of Environmental Sciences, Informatics and Statistics, University of Venice Ca' Foscari, Venice, Italy

Abstract

Estimating and interpreting ecosystem metabolism remains an important challenge in stream ecology. Here, we propose a novel approach to model, estimate, and predict multiseasonal patterns of stream metabolism (gross primary production [GPP] and ecosystem respiration [ER]) at the reach scale leveraging on increasingly available long-term, high-frequency measurements of dissolved oxygen (DO). The model uses DO measurements to estimate the parameters of a simple ecosystem model describing the underlying dynamics of stream autotrophic and heterotrophic microbial biomass. The model has been applied to four reaches within the Ybbs river network, Austria. Even if microbial biomasses are not observed, that is, they are treated as latent variables, results show that by accounting for the temporal dynamics of biomass, the model reproduces variability in metabolic fluxes that is not explained by fluctuations of light, temperature, and resources. The model is particularly data-demanding: to estimate the 11 parameters used in this formulation, it requires sufficiently long, for example, annual, time series, and significant scouring events. On the other hand, the approach has the potential to separate ER into its autotrophic and heterotrophic components, estimate a richer set of ecosystem carbon fluxes (i.e., carbon uptake, loss, and scouring), extrapolate metabolism estimates for periods when DO measurements are unavailable, and predict how ecosystem metabolism would respond to variations of the driving forces. The model is seen as a building block to develop tools to fully appreciate multiseasonal patterns of metabolic activity in river networks and to provide reliable estimations of carbon fluxes from land to ocean.

Lotic ecosystems are key components of the global carbon cycle. They transform and bury more than half of the lateral carbon flux from terrestrial ecosystems (Cole et al. 2007; Battin et al. 2008; Regnier et al. 2013). The river network conceptualization has now moved from the notion of a "pipeline," where transport of organic carbon from land to ocean dominates the processes, to the active ecosystem concept, where organic carbon is mineralized, buried, and/or transported (Battin et al. 2009; Trimmer et al. 2012). The key components of stream ecosystem metabolism are gross primary production (GPP), which is the carbon fixed through photosynthesis by primary producers (autotrophs) and ecosystem respiration (ER), which is the sum of the carbon respired by both heterotrophs and autotrophs (Tank et al. 2010). The prominent role in carbon cycling of microorganisms attached to stream sediments is acknowledged for headwater streams and low-order rivers (Naegeli and Uehlinger 1997; Battin et al. 2016), whereas microorganisms suspended in the water column may become more relevant in larger lowland rivers (Battin et al. 2008).

Modeling stream metabolism can be dated back to the 1950s when Odum (1956) introduced the open-water method, based on reach-scale diel oxygen mass balance techniques. Such method (*see*, e.g., Demars et al. 2015) model diel fluctuations of dissolved oxygen (DO) concentration in the water column as the balance between areal GPP, generally assumed to vary with light, ER, assumed constant throughout the day or temperature dependent, and reaeration that tends to equilibrate DO to saturation. The conceptual pathway usually followed when studying stream ecosystem metabolism consists of estimating daily GPP and ER from DO data and statistically relating these fluxes to environmental variables (e.g., light and nutrient availability, temperature, position in the river network) to unravel possible drivers and controls (*see*, e.g., Holtgrieve et al. 2010; Grace et al. 2015; Ulseth et al. 2018). An environmental variable often used in such analyses is the time elapsed since the last flood as a possible proxy of benthic microbial biomass (i.e., periphyton) (*see*, e.g., Uehlinger et al. 1996). Indeed, peak flow conditions can restructure or transiently perturb sedimentary habitats and their biofilms and thus, the related

*Correspondence: enrico.bertuzzo@unive.it

Additional Supporting Information may be found in the online version of this article.

ecosystem fluxes. At low densities of primary producers (i.e., periphytic algae and cyanobacteria), GPP is expected to increase proportionally to biomass; at higher densities, however, competition for space and resources could decelerate metabolic processes (McIntire and Phinney 1965; Roman and Sabater 1999; DeLong et al. 2014; Jäger and Borchardt 2018). The respiration of autotrophs and heterotrophs could also show similar density dependence effects at increasing biomass densities. Moreover, ecosystem metabolism and biomass dynamics are tightly coupled because positive net ecosystem production (NEP = GPP − ER) is stored, at least temporarily, in the form of biomass. Therefore, inter- and intra-annual patterns of stream metabolism possibly carry a signature of the underlying dynamics of microbial biomass.

Despite the natural link between ecosystem metabolism and microbial biomass, these two components have often been studied separately. Biomass dynamics is typically investigated in the context of riverine ecosystem models. Such classes of models range from complex setups, which seek to parameterize most of the processes deemed relevant to describe the major fluxes of energy and materials (e.g., McIntire 1973; McIntire and Colby 1978; Billen et al. 1994; Flipo et al. 2007), to more simple and parsimonious approaches (e.g., Uehlinger et al. 1996; Wootton et al. 1996; Uehlinger and Naegeli 1998; Acuña et al. 2008) that typically rely on direct measurements of biomass to evaluate their performances and/or estimate parameters. However, such measurements are costly and time consuming, especially if high-frequency (e.g., weekly) time-series are desired.

The goal of this article is to bridge the gap between metabolism and ecosystem models by proposing an approach that estimates metabolic fluxes based on high-frequency DO measurements by coupling oxygen dynamics with two additional nonobserved state variables describing the temporal evolution of autotrophic and heterotrophic benthic biomass. Specifically, the proposed model does not directly estimate daily GPP and ER based on DO data as traditionally done in open-water methods (but see Song et al. 2018, discussed also later). Rather, it infers critical ecosystem parameters controlling the underlying dynamics of autotrophic and heterotrophic biomass that would result in the observed long-term (e.g., annual), high-frequency (subdaily) time-series of DO concentration. The underlying assumption is that the interdaily variability of metabolic fluxes that is not explained by changes in light, temperature, and resources, can be, at least partially, explained by changes in biomass. We acknowledge, however, that specific (i.e., per unit biomass) metabolic rates can vary due to other factors, for example, community composition, disturbance, or simply a nonstationary behavior of the intrinsic rates. Such factors are currently not accounted for in our formulation which instead focuses on biomass as a first-order driver. Moreover, as a positive NEP implies an increase, at least temporarily, of biomass, an additional goal of the model is to track the fate of such biomass: that is, to estimate a seasonal pattern of biomass which is consistent with the observed DO (and thus metabolic) time series.

When short-term (i.e., from days to weeks and months) observations of DO are available, open-water methods still represent a most suitable tool to estimate ecosystem metabolism. However, recent developments in sensor technology have greatly increased the availability of long-term, high-resolution stream monitoring (Appling et al. 2018*b*; Bernhardt et al. 2018). In this scenario, we propose the framework developed herein as a complementary tool to trace a broader picture of the set of ecosystem processes driving seasonal variations of stream metabolism. This, however, comes at the cost of further assumptions which restrain the applicability and introduce limitations that will be carefully discussed.

While the general formulation of the proposed model can be applied to a spatially explicit framework of stream networks, the aim of this study is to develop the model at reach scale and to test it using existing data on ecosystem metabolism from a subalpine stream network (Ybbs river, Austria) (Ulseth et al. 2018). Particular attention has been given to the selection of an appropriate model structure to ensure the identifiability of parameters while providing a sufficient complexity to include the key processes controlling metabolism at reach scale.

This article is organized as follows. First, we describe the general model formulation. Then, we introduce our case study and detail the case-specific assumptions employed for the simulation of the tested reaches. The selected functional forms of the ecosystem fluxes are then illustrated followed by a description of the parameter estimation procedure. The last part of the article focuses on results, discussion, limitations, and possible future developments.

Theoretical approach

The proposed model assumes that the temporal dynamics of the ecosystem metabolism at reach scale is dominated by autotrophic and heterotrophic biomass not advected by the water flow that is biofilms attached to benthic and hyporheic sediments (Battin et al. 2016). The model is zero-dimensional as it assumes perfect mixing conditions and thus neglects spatial gradients within the control volume. The structural model describes the temporal dynamics of three state variables: autotrophic biomass B_A, heterotrophic biomass B_H (both expressed in mass units of carbon), and water volume V. In addition, a measurement model relates the state variables to the DO mass (and concentration) for which observations are available (see model conceptualization in Fig. 1). Mathematically, the model translates into four ordinary differential equations:

$$\begin{cases} \dfrac{dV}{dt} = Q_{up} + Q_L - Q & (1a) \\ \dfrac{dB_A}{dt} = P(B_A,\cdot) - R_A(B_A,\cdot) - L_A(B_A,\cdot) - S_A(B_A,\cdot) & (1b) \\ \dfrac{dB_H}{dt} = U(B_H,\cdot) - R_H(B_H,\cdot) - L_H(B_H,\cdot) - S_H(B_H,\cdot) & (1c) \\ \dfrac{d\mathrm{DO}}{dt} = \phi_{up} + \phi_L - \phi + \gamma_P P(B_A,\cdot) - \gamma_A R_A(B_A,\cdot) - \gamma_H R_H(B_H,\cdot) + R_e & (1d) \end{cases}$$

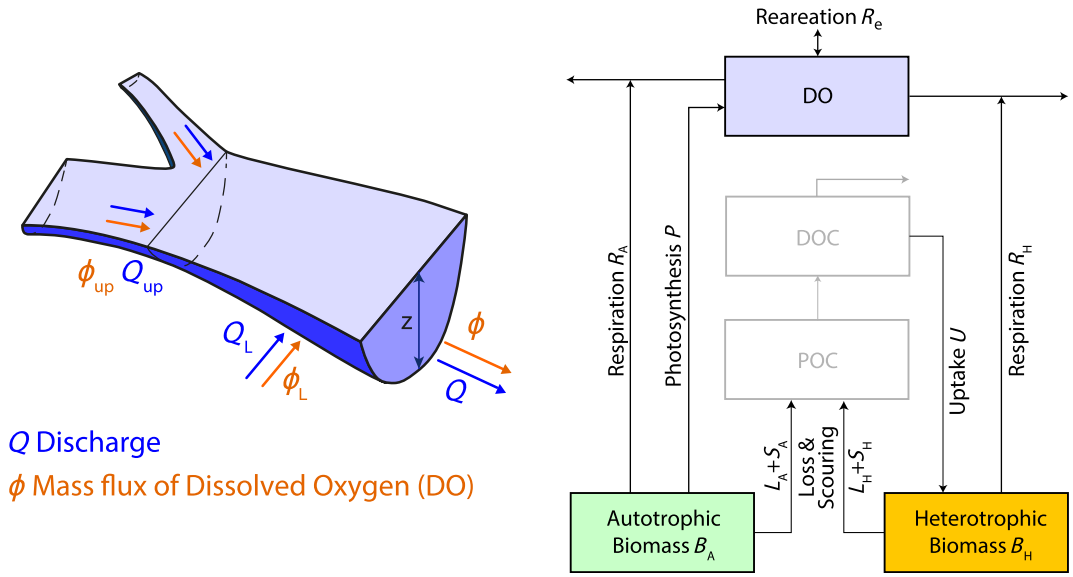

Fig. 1. Illustration of the theoretical approach. Left panel (partially adapted from Carraro et al. 2019) depicts the volumetric (blue) and mass (orange) fluxes contributing, respectively, to the reach scale water and DO balances (Eqs. 1a, 1d). Right panel focuses on the reach-scale ecosystem model and the bio-physical processes considered for the biomass evolution (Eqs. 1b, 1c). Beside the water volume, state variables, represented with colored boxes, are DO, autotrophic (B_A) and heterotrophic (B_H) biomass, respectively. Photosynthesis P, respiration R, uptake U, loss L, scouring S, and reaeration R_e represent the fluxes from pool to pool. Gray shaded variables, that is, dissolved organic carbon (DOC) and particulate organic carbon (POC), are not currently included in the model formulation but they are here proposed as the next model improvement to allow a spatially explicit, network-scale description of the process (*see* "Discussion" section).

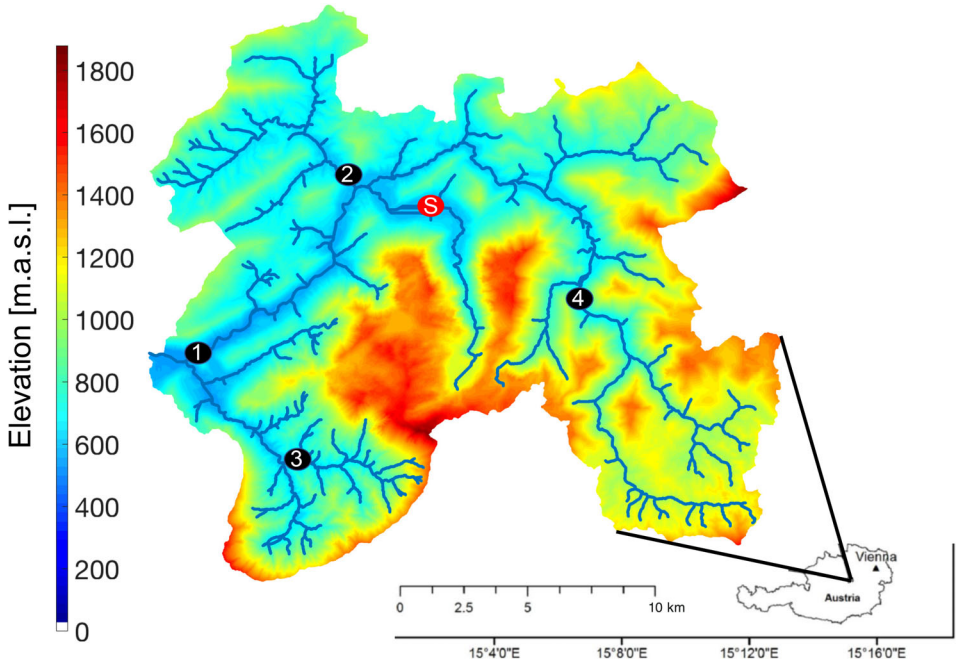

Fig. 2. The Ybbs river and its fluvial network extracted from a digital elevation model (catchment color displays elevation in m.a.s.l.). Black circles indicate the study site locations, numbered in ascending order according to their elevation, while the red dot locates the Lunz meteorological station.

where the dependence on the state variables B_A and B_H has been highlighted to stress the coupling between oxygen and biomass dynamics (see list of symbols and units in Table C1 in Appendix C). Water volume V (Eq. 1a) in the reach results from the balance among the input discharge from upstream Q_{up}, the lateral contribution Q_L, which lumps all hydrological

fluxes, such as snowmelt, surface and subsurface runoff, groundwater inflow, or recharge of the portion of the catchment directly drained by the focus reach, and the outflow discharge Q. Modeling the variations of water volume, and the underlying variations of channel geometry, allows us to explicitly account for the effects of hydrological fluctuations on DO concentration, reaeration, and biofilm disturbance.

Autotrophic biomass B_A (Eq. 1b) increases because of the net photosynthetic flux (P), representing the rate at which CO_2 is fixed into biomass. Biomass is lost through respiration (R_A), which is the carbon spent to subsidize all the maintenance processes using photosynthesis products, scouring (S_A), a flow induced process, as well as by a loss term (L_A), encapsulating mortality, detachment, grazing, and exudation, for instance. Heterotrophic biomass is conceptualized similarly (Eq. 1c), with the exception of the net influx, which is represented by carbon uptake (U).

The balance of DO is formulated in Eq. 1d. The first three terms at the right-hand side represent the hydrological advective fluxes of DO related to upstream (ϕ_{up}), lateral (ϕ_L), and outflowing (ϕ) discharges. As the model assumes well-mixed conditions (zero-dimensional assumption), the latter flux can be straightforwardly related to the other state variables as:

$$\phi(t) = Q(t)\frac{\mathrm{DO}(t)}{V(t)} = Q(t)[\mathrm{DO}](t) \quad (2)$$

where $[\mathrm{DO}](t)$ represents DO concentration [M L^{-3}] (square brackets are used to indicate elemental concentration throughout the article). The introduction of the γ weight conversion coefficients [M/M] from carbon to oxygen mass units allows for the direct coupling of the oxygen balance Eq. 1d with the photosynthetic and respiratory rates introduced in Eqs. 1b, 1c. Specifically, γ_P represents the photosynthetic quotient, which is the ratio between the mass of oxygen produced per unit mass of carbon fixed in the Calvin-cycle, whereas γ_A and γ_H are referred to the respiratory processes of autotrophs and heterotrophs, respectively. Such coefficients have been assumed constant and equal to $\gamma_P = \gamma_A = \gamma_H = 32/12$ (g O_2 g C^{-1}) (Bott et al. 1978; Burris 1981; Demars et al. 2016). The impact of this assumption and its relaxation are discussed later. Finally, the last term of Eq. 1d considers the gas exchange of DO across the air–water interface (R_e). Reaeration is driven by the difference between saturated and actual DO concentration, and by the oxygen transfer coefficient, which depends on hydraulic and hydrological conditions (Raymond et al. 2012; Palmeri et al. 2013).

Traditional open-water metabolism methods, for example, the single-station model (Wilcock et al. 1998), focus on Eq. 1d at a daily timescale and directly estimate GPP (in this formulation, GPP = $\gamma_P P(B_A, \cdot)$) and ER (ER = $\gamma_A R_A(B_A, \cdot) + \gamma_H R_H(B_H, \cdot)$) so that simulated oxygen concentration matches observed diel fluctuations. A notable exception is the work by Song et al. (2018) where the authors do not directly estimate GPP and ER but rather the parameters of functional forms that relate metabolic fluxes to light and temperature. Also in this case, however, the authors allow for a different parameter set for each individual day of analysis to account for the potential day-to-day variation of the relation between metabolic fluxes and environmental variables. The aim of our model is to explain such day-to-day variability focusing on biomass as a first-order control. Therefore, the proposed model relates production and consumption of oxygen (i.e., GPP and ER) to the ecosystem fluxes described in the structural model. The focus therefore switches to the estimation of the parameters controlling such fluxes so that the model simulation matches long-term (i.e., without applying the model separately to each day) high-frequency time series of observed DO concentration. We therefore hypothesize that such time series, together with ancillary information about environmental variables, such as temperature, discharge, and light, contain sufficient information to characterize the simple ecosystem model introduced herein. Moreover, as autotrophic and heterotrophic processes have different drivers, we hypothesize that it is potentially possible to infer the temporal dynamics of their biomass and to resolve their contribution to ER.

The specific functional form of the single terms of Eqs. 1b, 1c should be carefully considered depending on the case study and on the environmental data available, possibly selecting among different model formulations based on information criteria. Model formulations for carbon fluxes like photosynthesis, uptake, respiration, and loss processes generally involve the product between biomass and a specific rate. The latter is typically affected by temperature and other limiting factors (e.g., light, nutrient availability) and can depend on biomass through density dependent effects. The goal is to maintain a relatively simple formulation. Considering the two endpoints of the complexity spectrum of possible approaches to model stream ecosystem processes and metabolism, ranging from a comprehensive ecosystem model (e.g., McIntire and Colby 1978; Flipo et al. 2004), to the single-station method (e.g., Wilcock et al. 1998), our approach should be seen as a step starting from the latter toward the former, rather than vice-versa.

Study site

The Ybbs River network shown in Fig. 2 drains a 256 km^2 subalpine catchment in Austria (47°48′22.9″N, 14°57′00.8″E), with elevations ranging from 532 to 1831 m above sea level (m.a.s.l.). Calcareous dolomitic limestone is prominent throughout the catchment (*see*, e.g., Ceola et al. 2014; Ulseth et al. 2018). In this article, we focus on four study sites (Fig. 2, black circles). For each reach, high-frequency (5 min time step) measurements of DO concentration ([DO]), water temperature (T), and photosynthetically active radiation (PAR) are available for the period of January 2013–May 2014 (Ulseth et al. 2018). Barometric pressure (p) for each site was obtained from the measurements at the Lunz meteorological station (*see* Fig. 2) by correcting for elevation difference. Discharge

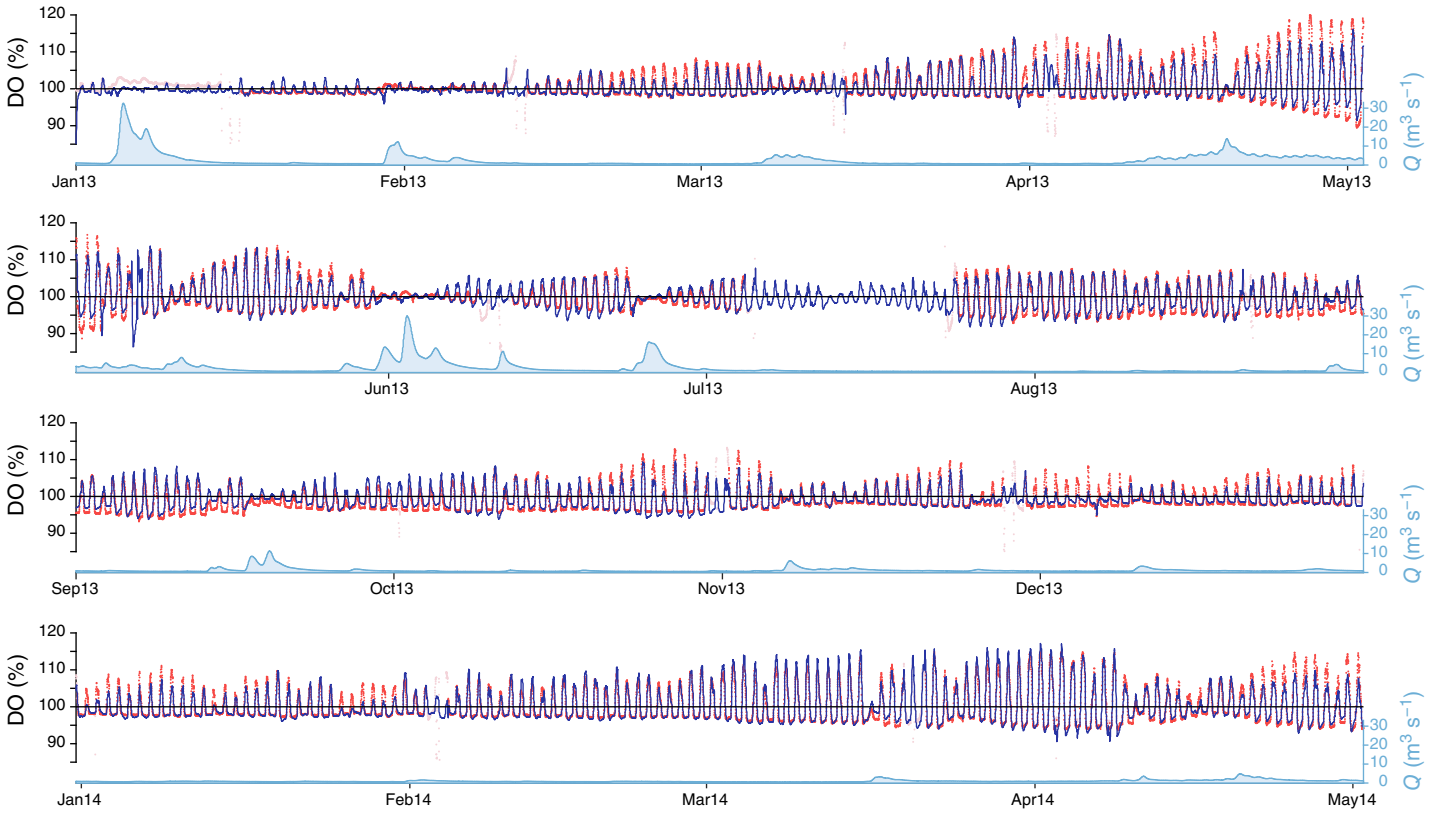

Fig. 3. Measurement model output. Plot of simulated DO series (expressed as relative to 100% saturation, blue solid line) against DO observations (red dotted line). Shaded red dots refer to data points excluded from the parameter estimation because either measurements of forcings were unavailable or DO sensor was being maintained. Baseline of 100% represents saturation conditions. Discharge measurements are also reported for the simulation period. Results refer to site 2. Larger figures for all four sites are reported in "Results" section Supporting Information.

Table 1. Study reaches geometry information.

			Site			
Feature	**Symbol**	**Units**	**1**	**2**	**3**	**4**
Elevation	h	m.a.s.l.	530	587	614	658
Width	w	m	25	10	5	10
Slope	s	‰	3.2	3.2	3.2	6.3
Roughness coefficient	K_s	$m^{1/3}s^{-1}$	15	14	25	14
Drainage area	a	km^2	203.8	34.6	46.4	16.2
Autotrophic density dependency	$K_{D,A}/A$	g C m^{-2}	20	70	7	15
Heterotrophic density dependency	$K_{D,H}/A$	g C m^{-2}	200	200	200	200

was measured at the outlet at an hourly time step and downscaled to the four study reaches by assuming local discharge proportional to contributing area. In addition, monthly grab samples of benthic chlorophyll *a* (Chl *a*) and ash-free dry mass (AFDM) were collected.

Dissolved organic carbon (DOC) concentration is not available for all the study sites and periods. However, Fasching et al. (2016) studied DOC dynamics in the Ybbs catchment and reported strong hydrological controls over patterns in concentration. Accordingly, [DOC] can be approximated by a power law relationship of the type: $[\mathrm{DOC}](t) = \alpha_Q + \beta_Q(Q(t))^{\gamma_Q}$. Other site geometry information collected through previous studies (Ceola et al. 2014; Ulseth et al. 2018) are summarized in Table 1.

Model application

Similar to the single-station model, we assumed that ecosystem processes in the focal reach are representative of the

dynamics of a sufficiently long stream segment so that upstream DO concentration is comparable to that in the study reach. Moreover, as the study reaches have a sufficiently large drainage area (*see* Table 1), it can be assumed that lateral flow is negligible compared to the upstream contribution ($Q_L \ll Q_{up}$ and $\phi_L \ll \phi_{up}$). The reach cross-section geometry is approximated with rectangular shape of constant width w. Water depth $z(t)$ is estimated assuming uniform flow condition via the Manning's equation: $Q(t) = wz(t)K_s r(t)^{2/3}\sqrt{s}$, where r indicates the hydraulic radius, that is, the ratio of the cross-sectional area to the wet perimeter, which for rectangular cross-sections reads $r = w \cdot z/(w+2z)$. See other parameters in Table 1.

We tested several different model formulations for the single terms of Eqs. 1a–1d. In particular, as experiments have shown evidence of density dependent effects, that is, photosynthesis and related processes diminish with increasing biomass (*see*, e.g., McIntire and Phinney 1965; Roman and Sabater 1999; DeLong et al. 2014), we focused on testing model formulations with different combinations of density dependent effects applied to photosynthesis, carbon uptake, respiration, and death (*see* "Methods" section in Supporting Information). Model selection was performed via Akaike's information criterion (AIC, Burnham and Anderson 2003, see also "Methods" section in Supporting Information).

Table 2. Model assumptions. Numbers in brackets refer to the number of parameters the specific flux introduces to the model formulation.

Model assumptions	
General model assumptions:	
• Benthic and hyporheic biofilms dominate ecosystem metabolism	
• Zero-dimensional model/perfect mixing	
• $\gamma_P = \gamma_A = \gamma_H$ = 32/12 g O_2 g C^{-1}	
Specific case study model assumptions:	
• Rectangular cross-section of constant width	
• Uniform flow conditions	
• $Q \propto a$	
• $Q_L \ll Q_{up}$	
• $\phi_L \ll \phi_{up}$	
• $\phi_{up} = Q_{up}[DO]_{up} \simeq Q_{up}[DO]$	
• [DOC] = $f(Q)$	
Functional dependencies of the selected model:	
• P: density-dependent and limited by PAR and T	[3]
• U: density-dependent and limited by [DOC] and T	[2]
• R_H and R_H: density-dependent and limited by T	[2]
• L_A and L_H: linear with biomass	[2]
• S_A and S_H: linear with biomass and quadratic function of τ	[2]
• R_e: K_{DO} calculated according to eq. 1 in table 1 of Raymond et al. (2012)	
Total number of parameters	**11**

Table 2 provides a synthetic summary of all model assumptions and the formulation of the most informative model, which is further detailed in what follows. For a complete overview of the other formulations tested, see "Methods" section in Supporting Information.

Photosynthesis

Net carbon fixation rate, $P(t)$, is modeled as a function $P(t) = f(\mathrm{PAR}(t), T(t), B_A(t))$, accordingly to the following equation:

$$P(t) = \mu_{P,20} f_{T,L}(t) B_A(t) \left(1 - \frac{B_A(t)}{K_{D,A}}\right) \tag{3a}$$

$$f_{T,L}(t) = \theta_A^{T(t)-20} \frac{\mathrm{PAR}(t)}{\mathrm{PAR}(t) + K_{\mathrm{PAR}}} \tag{3b}$$

where $\mu_{P,20}$ [T^{-1}] represents the specific photosynthetic rate at standard temperature conditions (T = 20°C) without light limitation; $f_{T,L}$ quantifies the effect of temperature and light. The former is modeled trough the classical exponential Arrhenius model (Jørgensen and Bendoricchio 2001). Light dependence typically shows a saturation effect, if photoinhibition is neglected (*see*, e.g., Jassby and Platt 1976), and it is here modeled through a Michaelis–Menten curve where K_{PAR} [J L^{-2}] represents the local half saturation concentration (Uehlinger et al. 1996). A density dependent term ($1 - B_A(t)/K_{D,A}$) linearly decreases the photosynthetic rate as biomass B_A increases according to the parameter $K_{D,A}$ [M]. We acknowledge the relevance of nutrients for ecosystem metabolism. However, the lack of highly resolved measurements of nutrients prevents their explicit inclusion in the model.

Carbon uptake

Model formulation for heterotrophic carbon uptake follows the same rationale as for autotrophic carbon fixation rate as shown in the following equation:

$$U(t) = \mu_{U,20} f_{T,\mathrm{DOC}}(t) B_H(t) \left(1 - \frac{B_H(t)}{K_{D,H}}\right) \tag{4a}$$

$$f_{T,\mathrm{DOC}}(t) = \theta_H^{T(t)-20} \frac{[\mathrm{DOC}](t)}{[\mathrm{DOC}]_{\max}} = \theta_H^{T(t)-20} \frac{\delta_Q + Q^{\gamma_Q}}{\delta_Q + Q_{\max}^{\gamma_Q}} \tag{4b}$$

where $\mu_{U,20}$ [T^{-1}] represents the reference uptake rate at standard temperature and maximum DOC concentration. The density-dependent term models the slowdown of the maximum uptake rate (e.g., as a result of resource competition) as biomass increases. Temperature dependence is again exponential of θ_H [–] parameter. The other main factor controlling the uptake rate is DOC concentration, which is assumed to linearly control the uptake rate as shown in Eq. 4b, thus reflecting the simple assumption that the higher the food availability the higher the uptake rate. More complex interactions could have been considered (e.g., a saturation function, a linear/

saturation function coupled with an explicit intracellular carbon storage modeling). However, due to the limited range of observed DOC fluctuations as well as the high heterogeneity of organisms and DOC composition at reach scale, we resort to the simplest linearized formulation to avoid overparameterization of such a process. High DOC concentrations do not lead to an unconstrained uptake rate because of the density-dependent term, and therefore we assumed an indirect saturating effect. We estimated DOC at the reach scale relying on the empirical relationship found by Fasching et al. (2016) for the study catchment, that is, $[\mathrm{DOC}](t) \propto Q(t)$ or $[\mathrm{DOC}](t) = \alpha_Q + \beta_Q Q^{\gamma_Q}(t)$. Such a relationship implies that maximum DOC concentration is reached at maximum discharge. We defined $\delta_Q = \alpha_Q/\beta_Q$ and according to Fasching et al. (2016), we posed δ_Q and γ_Q, respectively, equal to 4.7 and 0.4, assuming an average DOC-Q relationship during the rising and falling limb of the hydrograph.

Respiration

Respiration for both autotrophs (R_A) and heterotrophs (R_H) is modeled as a density-dependent, temperature-driven, dynamic process:

$$R_A(t) = \mu_{R,A,20}\theta_A^{T(t)-20}B_A(t)\left(1-\frac{B_A(t)}{K_{D,A}}\right) \quad (5a)$$

$$R_H(t) = \mu_{R,H,20}\theta_H^{T(t)-20}B_H(t)\left(1-\frac{B_H(t)}{K_{D,H}}\right) \quad (5b)$$

where, for model parsimony, temperature- and density-dependent parameters (θ and K_D) regulating respiration are assumed to be equal to those controlling photosynthesis and uptake for autotrophs and heterotrophs, respectively.

Note also that the current model formulation correctly reproduces the feature that net growth rate, defined as photosynthesis (or carbon uptake for heterotrophs) minus respiration, is not strictly positive. For instance, during night $f_L = 0$ and thus $R_A > P$, implying that autotrophs loose biomass because of maintenance metabolism. Similarly, for very low DOC concentration, $R_H > U$, implying that energy sources for heterotrophs may switch to the internal carbon storage.

Table 3. Setup of the Monte Carlo calibration*.

Parameter	Symbol	L.B.	U.B.
A. Temperature dependence factor	θ_A	1	2
H. Temperature dependence factor	θ_H	1	2
Light half saturation concentration	K_{PAR}	10^3	10^5
Photosynthetic rate	$\mu_{P,20}$	0	5
A. Respiration rate	$\frac{\mu_{R,A,20}}{\mu_{P,20}f_{L,\max}}$	10^{-3}	0.6
A. Loss rate	$\frac{\mu_{L,A}}{(\mu_{P,20}f_{L,\max}-\mu_{R,A,20})f_{T,\max}}$	10^{-3}	0.5
Uptake rate	$\mu_{U,20}$	0	10
H. Respiration rate	$\frac{\mu_{R,H,20}}{\mu_{U,20}}$	10^{-2}	0.9
H. Loss rate	$\frac{\mu_{L,H}}{(\mu_{U,20}-\mu_{R,H,20})f_{T,\max}}$	10^{-3}	0.5
Scouring rate	μ_S	0	250
Min shear stress to initiate scouring	τ_0	0	150

L.B., lower bound; U.B., upper bound.
*A: Autotrophic; H: Heterotrophic; Names refer to the target parameter.

Loss and scouring

Biomass is assumed to leave the system by means of loss processes and detachment induced by scouring. Loss is modeled through a simple linear dependence:

$$L_A(t) = \mu_{L,A}B_A(t) \quad (6a)$$

$$L_H(t) = \mu_{L,H}B_H(t) \quad (6b)$$

where $\mu_{L,A}$ and $\mu_{L,H}$ represent the specific biomass loss rates for autotrophs and heterotrophs, respectively, including all processes not directly linked to stormflow, such as mortality, detachment, predation, exudation, or viral lysis. Streamwater temperature can induce loss through microbial cell mortality. However, such effects become apparent at very high or low temperatures only and we therefore assumed a constant loss rate for the sake of simplicity. Density-dependent effects on loss rates have not been retained during model selection (*see* "Methods" section in Supporting Information). After model selection, therefore, the formulation that best explains the data assumes that photosynthesis, uptake, and respiration slow as density increases according to parameters $K_{D,A}$ and $K_{D,H}$. Notice that these parameters do not represent the carrying capacities of the system because the equilibrium biomass is reached for values $B < K_D$ at which gross production balances respiration and loss (see detailed calculation in Appendix A).

Hydrological disturbance quantified by bottom shear stress τ [M L^{-1} T^{-2}] is a major factor limiting biomass accrual (*see*, e.g., Uehlinger et al. 1996; Acuña and Tockner 2010; Bellmore et al. 2014) and has therefore been explicitly modeled. Under the assumption of uniform flow conditions, τ is equal to the product between the hydraulic radius r [L], the specific weight of water γ_w [M L^{-2} T^{-2}], and the channel slope s [–] (Eq. 7d). The scoured biomass per unit time (S_A and S_H) is expressed as a function of the excess of shear stress from the minimum necessary to initiate the process, as illustrated in Eqs. 7a–7d:

$$S_A(t) = \mu_S f_S(t)B_A(t) \quad (7a)$$

$$S_H(t) = \mu_S f_S(t)B_H(t) \quad (7b)$$

$$f_S(t) = \left(\frac{\tau(t)-\tau_0}{\tau_{\max}-\tau_0}\right)^2 \quad \tau(t) \geq \tau_0 \quad (7c)$$

$$\tau(t) = \gamma_w r(t) s \quad (7d)$$

where μ_S [T^{-1}] is the specific sloughing rate, modulated by the f_S term which is a quadratic function of the ratio between the

actual excess of shear stress ($\tau - \tau_0$) from the minimum force needed to activate the process (τ_0) to the maximum excess experienced ($\tau_{max} - \tau_0$). Even though heterotrophs dominate the hyporheic zone whereas autotrophs are confined to the benthic zone, at ecosystem scale, scouring and bed movement are here assumed to occur at the same rate (μ_S) for both B_A and B_H.

Reaeration

The reaeration flux $R_e(t)$ [M T^{-1}] was modeled, considering the low solubility of oxygen and its high abundance in the atmosphere (i.e., its atmospheric partial pressure is almost constant and can be substituted with its saturation concentration in water [DO_{sat}]), as follows:

$$R_e(t) = K_{DO}(t)\left([DO]_{sat}(t) - [DO](t)\right)V(t) \quad (8)$$

where K_{DO} [T^{-1}] represents the oxygen transfer coefficient (Palmeri et al. 2013). K_{DO} is computed accordingly to eq. 1 in table 1 of Raymond et al. (2012) and validated by the nighttime regression approach ("Methods" section in Supporting Information). A compendium of the formulae adopted for $[DO]_{sat}$ and K_{DO} is reported in the "Methods" section in Supporting Information.

Parameter estimation

The model (1a–1d) is solved numerically using a forward Euler scheme. Parameter estimation is done for each site separately. The time resolution of Δt = 15 min was chosen to ensure the stability and accuracy (compared to higher order schemes) of the numerical scheme in a reasonable computational time while exploiting the potential of the high-frequency measurements.

Model parameters were set a priori when available from field surveys or previous work (Fasching et al. 2014; Schelker et al. 2016; Ulseth et al. 2018) and are summarized in Table 1. The remaining 11 free parameters (Table 3) were estimated in a Bayesian framework. Specifically, we used the $DREAM_{ZS}$ (Ter Braak and Vrugt 2008; Vrugt et al. 2009) implementation of the Markov Chain Monte Carlo (MCMC) algorithm. Parameter estimation was performed against relative oxygen concentration ($DO_{\%}(t) = 100 \cdot [DO](t)/[DO]_{sat}(t)$) assuming independent and identically distributed (IID) Gaussian errors. As not all parameter combinations lead to physically or biologically meaningful model trajectories, we specified some parameters as combination of other parameters or variables (Table 3). Such a choice (detailed in Appendix A) allows setting biologically meaningful ranges for the uniform prior distributions. To avoid the estimation of the initial conditions, we ran a 3-yr long model spin-up period forced with synthetic data obtained by replicating, on an annual basis, the observed environmental variables (i.e., discharge, light, water temperature, barometric pressure). For each site, we ran 2.5×10^6 iterations of the MCMC and estimated the parameter posterior distribution after the burn-in phase (around 3×10^5 iterations to reach chain convergence).

During preliminary tests, we found that the density-dependent parameters K_D were correlated with the rate parameters μ (e.g., for autotrophs, $K_{D,A}$ correlated with $\mu_{P,20}$, $\mu_{R,A,20}$, $\mu_{L,A}$). Indeed, such a correlation is expected given the structure of the model and the fact that DO is the only observed variable in the system (see detailed analysis in Appendix B). Simplifying the issue, K_D parameters set the order of magnitude of the respective biomass. If one doubles K_D and halves the rates for instance, the biomass approximately doubles but the carbon fluxes, which in turn control the dynamics of DO, remain approximately constant as they depend on the product of biomass and the specific rates. To avoid such over-parameterization, we decided to set $K_{D,A}$ and $K_{D,H}$ to realistic values and focus the analysis on the relative biomass (i.e., $B^* = B/K_D$). We estimated $K_{D,A}$ from site specific measurements of AFDM (*see* "Methods" section Supporting Information), while a reference value $K_{D,H}$ was estimated based on potential surface area, following the procedure described in Battin et al. (2016) ("Methods" section Supporting Information). It is worth noting that uncertainty in the estimation of K_D parameters would limit the possibility of estimating the absolute value of biomass from measurements of only DO. However, the estimation of metabolic processes and related carbon fluxes—the focus of our study—depends on the product between biomass and specific rates, and is not impaired.

Single-station comparison

To assess the plausibility of model results, we compared daily GPP and ER derived from our model with those estimated through the single-station method:

$$\frac{d[DO](t)}{dt} = \frac{1}{z(t)}\left[GPP_d\frac{PAR(t)}{PAR_d} - ER_d\right] + K_{DO}\left([DO]_{sat}(t) - [DO](t)\right) \quad (9)$$

This formulation (*see*, e.g., Van de Bogert et al. 2007; Hotchkiss and Hall 2014; Hall et al. 2015) assumes daily GPP (GPP_d, [ML^{-2} T^{-1}]) linearly varying with PAR (scaled by the averaged light intensity for day d and termed PAR_d [J L^2]), and daily ecosystem respiration (ER_d, [ML^{-2} T^{-1}]) constant throughout the day. Normalization by water depth (z) gives the required volumetric fluxes balancing the oxygen reaeration rate. Equation 9 was applied using the same water depth, saturation concentration, reaeration coefficient, time step, and numerical scheme used in our model. Estimation was performed assuming Gaussian IDD errors.

Results

Parameter estimation

The model reproduced fairly well seasonal and subdaily features of the observed high-resolution dynamics of DO

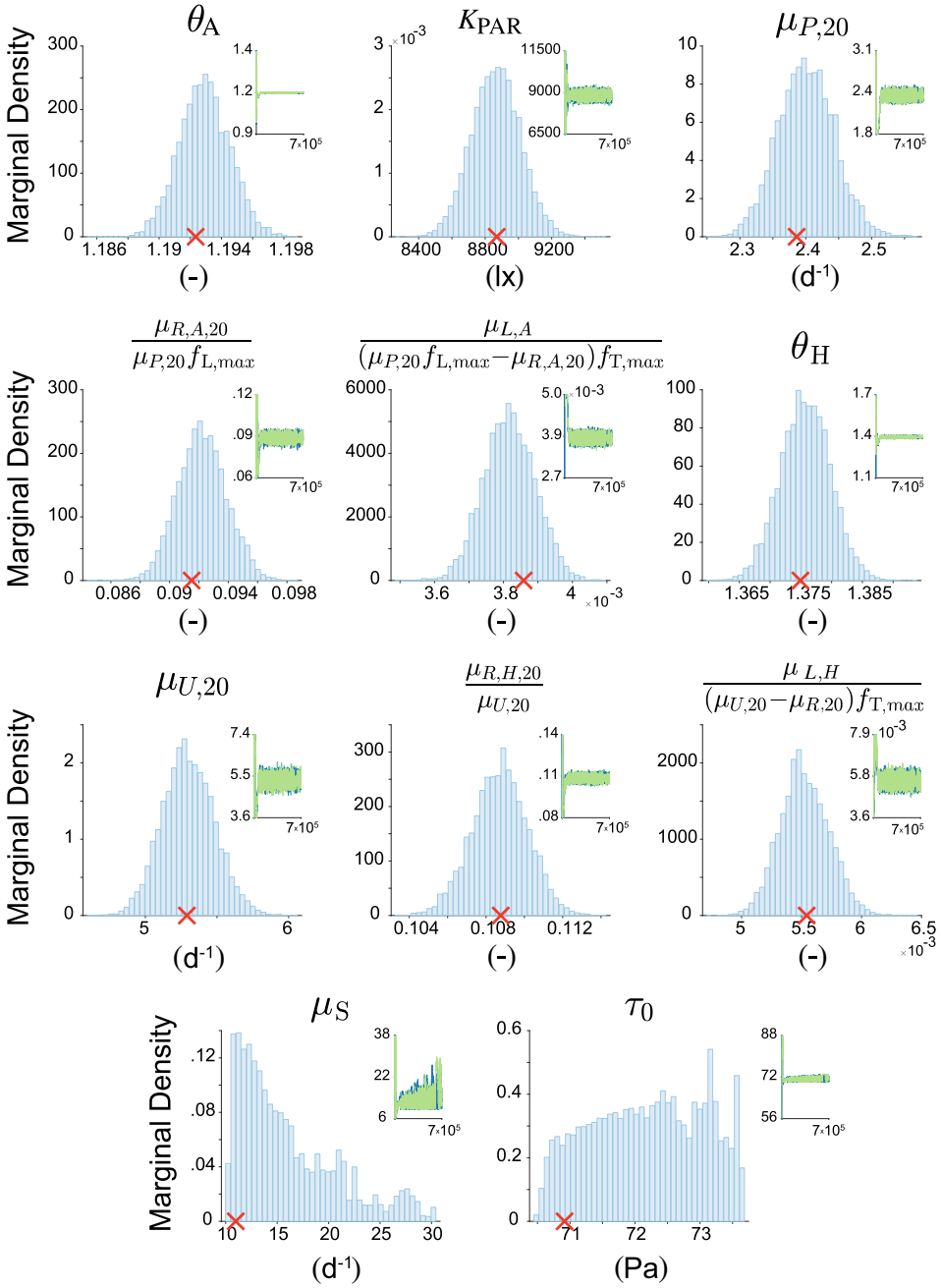

Fig. 4. Posterior distributions of model parameters and MCMC algorithm evolution. Light blue histograms show the marginal distributions sampled after the burn-in phase; red crosses highlight the parameter set with the highest likelihood. Inset plots illustrate for each parameter the whole evolution of the Markov Chain triplets and their region of convergence. Results refer to site 2. Larger figures for all four sites are reported in "Results" section in Supporting Information.

concentration (Fig. 3 for site 2, other cases are reported in "Results" section in Supporting Information). Particularly, the model is able to capture DO variations coinciding with streamflow peaks and attributable to an increase in reaeration or to a decrease in biomass owing to streambed scouring. Model performance, measured as the root mean square error (RMSE), reached on average, for best parameter sets, 1.58% (Table 4). The MCMC algorithm converged to a posterior distribution which spans a parameter region much narrower than that of the uniform prior (Fig. 4 and Table 4). Comparisons of between chains and within chains variances for each parameter were also checked using the diagnostic test of the R_c statistic of Gelman and Rubin (1992). All study sites reached $R_c < 1.2$, implying that convergence has been achieved.

Table 4. Summary of the MCMC parameter estimation procedure*.

		Site 1	Site 2	Site 3	Site 4
θ_A	–	1.036 (± 0.003)	1.192 (± 0.002)	1.121 (± 0.003)	1.076 (± 0.002)
K_{PAR}	lx	7549 (± 160)	8868 (± 146)	1245 (± 56)	4399 (± 59)
$\mu_{P,20}$	d^{-1}	1.82 (± 0.07)	2.39 (± 0.04)	0.91 (± 0.04)	2.53 (± 0.06)
$\mu_{R,A,20}$	d^{-1}	0.142 (± 0.006)	0.209 (± 0.006)	0.0010 ($\pm 9.4 \times 10^{-4}$)	0.0034 ($\pm 1.2 \times 10^{-4}$)
$\mu_{L,A}$	d^{-1}	0.0832 ($\pm 9.1 \times 10^{-4}$)	0.0052 ($\pm 5.3 \times 10^{-4}$)	0.0334 ($\pm 4.2 \times 10^{-4}$)	0.0785 ($\pm 4.9 \times 10^{-4}$)
θ_H	–	1.091 (± 0.004)	1.374 (± 0.004)	1.092 (± 0.001)	1.015 (± 0.001)
$\mu_{U,20}$	d^{-1}	0.437 (± 0.020)	5.173 (± 0.200)	0.251 (± 0.004)	0.515 (± 0.020)
$\mu_{R,H,20}$	d^{-1}	0.045 (± 0.001)	0.56 (± 0.02)	0.0344 ($\pm 1.5 \times 10^{-4}$)	0.0420 ($\pm 9.1 \times 10^{-4}$)
$\mu_{L,H}$	d^{-1}	0.042 (± 0.003)	0.0110 ($\pm 2.4 \times 10^{-4}$)	0.0313 ($\pm 7.1 \times 10^{-4}$)	0.1954 ($\pm 7.9 \times 10^{-4}$)
μ_S	d^{-1}	13.5 (± 22.2)	16.2 (± 4.8)	0.7 (± 64.3)	0.51 (± 0.02)
τ_0	Pa	116.7 (± 2.2)	72.5 (± 0.9)	49.1 (± 1.7)	10.4 (± 1.1)
$RMSE_{DO\%}$†	%	2.8226	1.6187	0.8575	1.0163
$RMSE_{DO\ -\ SS\%}$†	%	1.62486	1.2142	0.4565	1.0018

*Values refer to maximum a posteriori parameter sets, while standard deviations are reported between parenthesis.
†Root mean square errors of the proposed model (Eq. 1d) and the single-station model application (Eq. 9), respectively.

Moreover, multiple $DREAM_{ZS}$ runs were launched in parallel to check reproducibility of the results. The parameter posterior distribution converged to the same region in all cases.

Biomass dynamics and ecosystem metabolism

While Fig. 3 focuses on the performance of the measurement model, Figs. 5, 6 highlight the information that can be extracted from the structural model. Chief among them are the dynamics of autotrophic and heterotrophic biomass along with the corresponding time-series of daily GPP, ER, partitioned into its autotrophic and heterotrophic components, and NEP for all four study sites.

Although it is not possible to assess whether the predicted temporal dynamics of the biomass matches the real evolution due to the absence of direct observations, it is nonetheless interesting to analyze how, according to the model formulation and assumptions, autotrophic and heterotrophic biomass should evolve in order to reproduce the observed patterns of DO. Although the temporal dynamics of biomass presents characteristics specific to each site, it also broadly exhibits similar seasonal patterns. As autotrophic growth is driven by PAR and temperature, the most favorable conditions were met in late spring and early summer. Similarly, temperature plays a key role for the heterotrophic dynamics, whose temporal pattern is also primarily modulated by DOC availability, which in turn depends on discharge as we used Q as proxy for the DOC concentration. Consequently, in spring, increasing temperature and more frequent high-discharge events—increasing terrestrial deliveries of DOC according to our model assumptions—enhanced the development of heterotrophic biomass. In fall, however, lower temperatures and prolonged baseflow conditions lowered the equilibrium biomass that the ecosystem was able to sustain with its resources (*see* Appendix B). Biomass removal by scouring could locally perturb this seasonal pattern, but with different sensitivities for each reach (*see*, e.g., January 2013 flood event, Figs. 5, 6).

A site comparison of the annual cumulative values of GPP, ER, and NEP, expressed as g O_2 m^{-2}, is given in Table 5. Site 1 was most productive in terms of GPP (1216 g O_2 m^{-2}) and ER (977 g O_2 m^{-2}). Site 2 and 3 were seasonally more reactive with metabolism peaking in late spring and beginning of summer; however, their metabolic dynamics were substantially different. While site 2 saw an increase in both autotrophic production and heterotrophic respiration, with GPP~ER in spring, site 3 was characterized by lower autotrophic biomass ($K_{D,A}$ = 7 g C m^{-2} and $\mu_{P,20}$ = 0.914 d^{-1}), whose C fixation was outperformed by heterotrophic growth, and, as a result, by heterotrophic respiration (NEP < 0, $K_{D,H}$ = 200 g C m^{-2} and $\mu_{U,20}$ = 0.251 d^{-1}). Site 4, the highest in elevation, was weakly heterotrophic ecosystem (NEP < 0), respiring, over the entire simulation period, more than 800 g O_2 m^{-2} and producing almost the same amount.

Comparison with single-station model estimates

The overall magnitude and seasonal patterns of the simulated daily ecosystem metabolism is in approximate agreement with the single-station estimates (Figs. 5c, 6c, Table 4). Over the entire period, an averaged correlation coefficient of 0.75 (based on NEP covariance analysis) was obtained (R_{NEP}, Table 5). Discrepancies were mainly attributable to different dynamics estimated during high discharge. However, we argue that under such conditions, our model can possibly provide a more reliable estimate (*see* "Discussion" section). Another possible source of short-term deviations between the two approaches can be attributed to external variables that are not accounted for in model. This is the case, for instance, of the peak in GPP in spring 2014 in study site 1, estimated using the single-station approach but not reproduced by the model

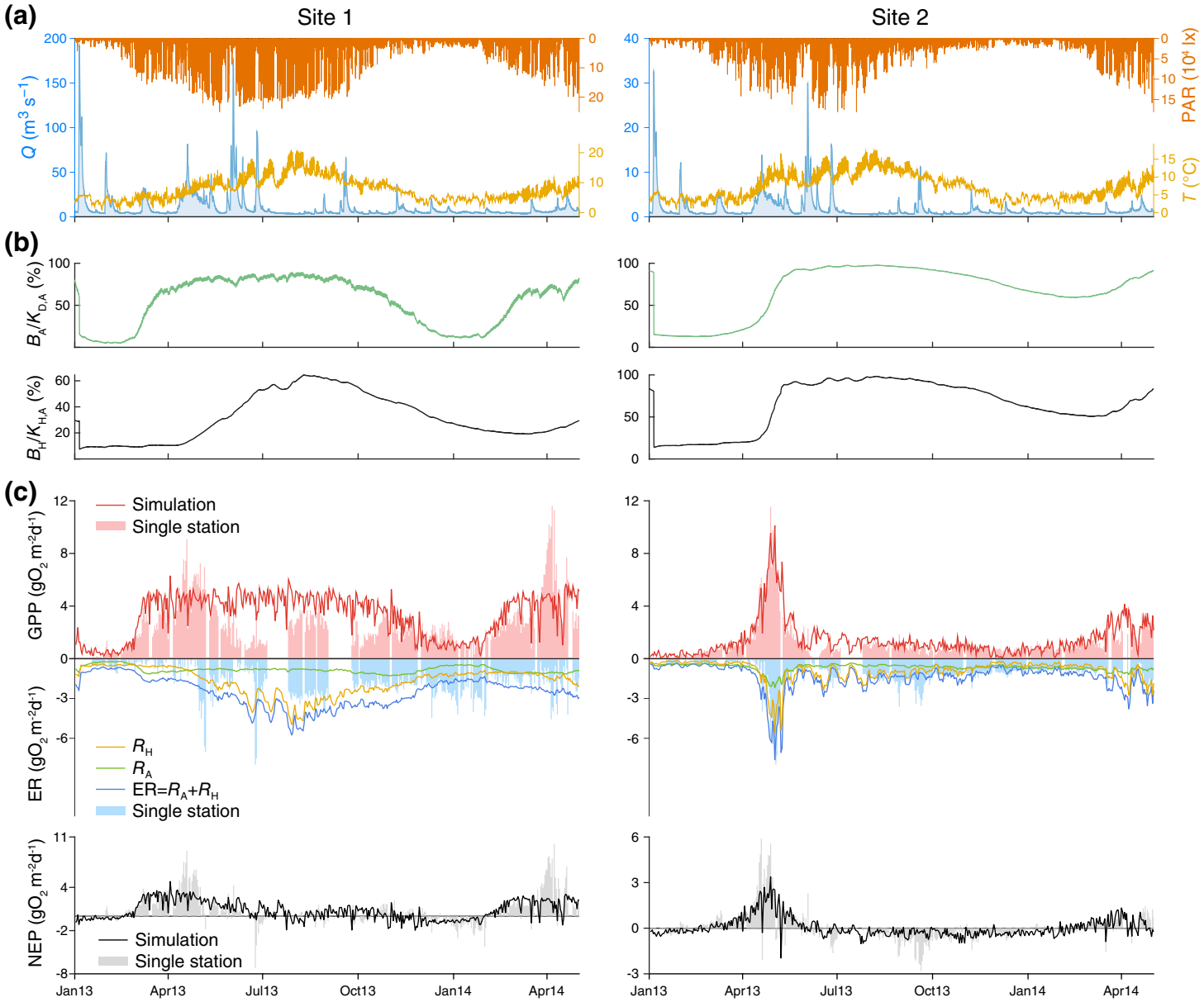

Fig. 5. Ecosystem metabolism for site 1 and site 2. (**a**) Time-series of PAR, temperature (T), and discharge (Q) drive the (**b**) temporal evolution of the simulated autotrophic (B_A) and heterotrophic (B_H) biomass, represented as normalized by the density dependence term K_D. (**c**) Simulated daily photosynthetic and respiratory fluxes: GPP (solid red line), ER (solid blue line), sum of the autotrophic (green) and heterotrophic (yellow) contributions and net ecosystem production, NEP = GPP − ER (black line). Single-station estimates are reported in shaded bars.

(Fig. 5c). A detailed study of the metabolic regime in this catchment attributed this peak to a flush of nutrients related to snowmelt (Ulseth et al. 2018). Obviously the model cannot reproduce such features as it does not account, at the moment, for nutrients dynamics.

Autotrophic and heterotrophic respiration

The proposed model is potentially able to resolve the autotrophic and heterotrophic contributions to ER. These two contributions have been clearly identified for study sites 1 and 2 (Fig. 5c). However, the predicted autotrophic respiration for study sites 3 and 4 was close to zero as the estimation procedure identified a parameter set which was able to explain DO concentrations relying only on heterotrophic respiration (*see* "Discussion" section for a detailed analysis).

Carbon fluxes

Although the present work primarily focuses on metabolic fluxes, a side asset of the structural model that accounts also for biomass dynamics is the possibility to track a richer set of

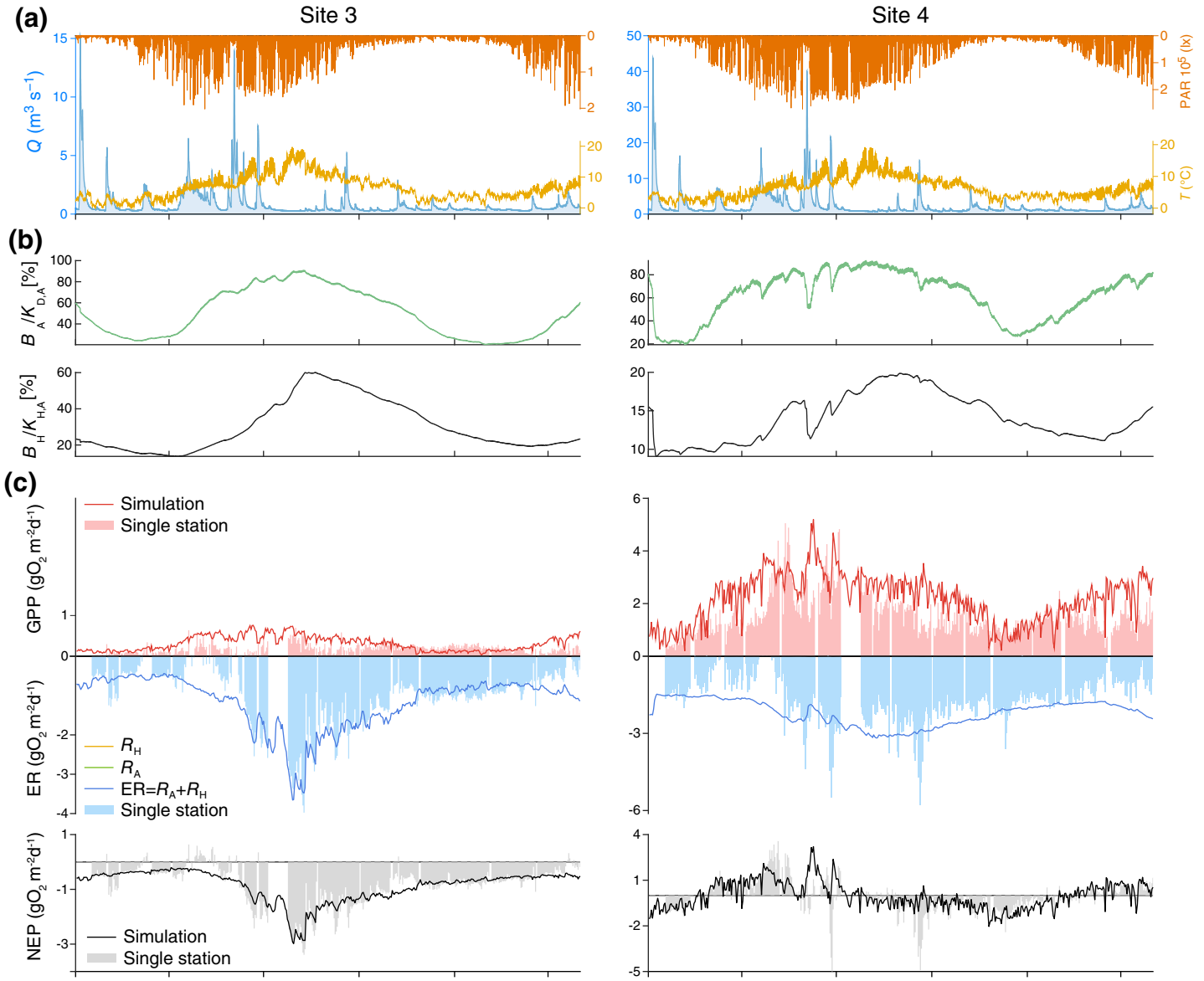

Fig. 6. Ecosystem metabolism for site 3 and site 4. Symbols as in Fig. 5.

carbon fluxes. Even though fluxes that do not have a direct impact on oxygen (i.e., uptake, loss, scouring) are more uncertain because of the lack of direct biomass observations, it is worth analyzing the carbon fluxes that simulate the biomass dynamics, which in turn explain, according the model assumptions, metabolic patterns. Figure 7 shows the estimated ecosystem carbon fluxes derived from tracking the fate of the carbon fixed into biomass (through either uptake or photosynthesis) and how it is partitioned in the output fluxes throughout the simulation window (January 2013–May 2014). Heterotrophy dominated ecosystem metabolism in all study reaches. Indeed, between 73% and 95% (left column for each site, orange bar) of the total carbon was fixed into biomass by heterotrophic microorganisms. The remaining fraction (left columns, red bar) was photosynthesized CO_2. The respiration flux (green and light orange bars) was lower than the sum of the loss (light blue and blue bars) and scouring (magenta and purple bars) terms. Disentangling the latter flux, loss rather than scouring was the dominant corridor for biomass removal. Indeed, scouring was acting, in most of the simulated sites, during extreme discharge events that were rather rare during the observation period.

Discussion

The framework developed in this article aims at modeling, estimating, and predicting stream metabolism. We do this by coupling metabolic fluxes with state variables describing the

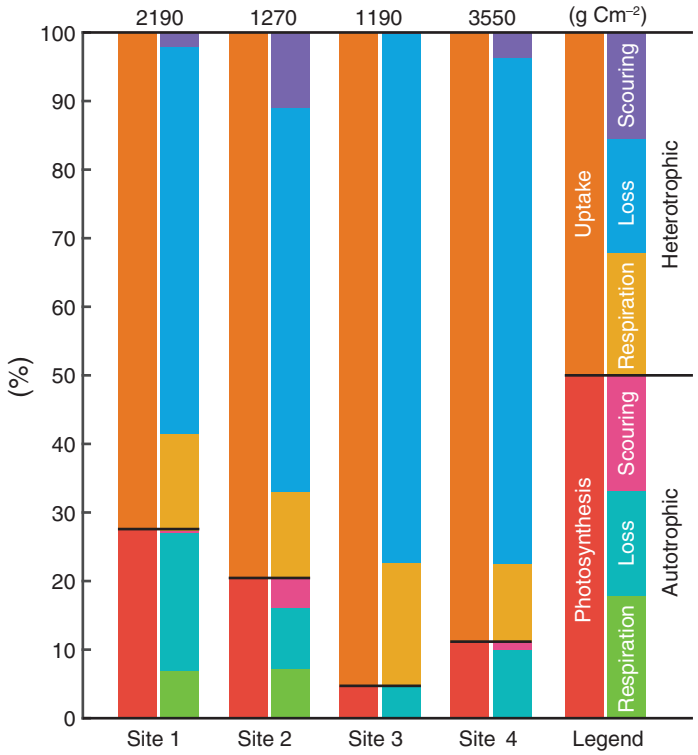

Fig. 7. Repartition of the modeled C fluxes throughout the entire simulation period (January 2013–May 2014). The total amount of carbon fixed into biomass throughout the simulation is reported on top of the bars. Left column for each site represents the proportion between the carbon photosynthesized and fixed through uptake by living organisms (positive terms in Eqs. 1b, 1c); right column shows how the fixed carbon is lost via respiration, loss processes, and scouring (negative terms in Eqs. 1b, 1c).

Table 5. Annual ecosystem metabolism.

Site		1	2	3	4
GPP	g O_2 m^{-2}	1216.0	492.7	121.9	812.1
ER	g O_2 m^{-2}	976.9	492.3	471.6	837.4
NEP	g O_2 m^{-2}	239.05	0.36	−349.7	−25.4
R_{NEP}	–	0.70	0.81	0.86	0.62

temporal dynamics of benthic and hyporheic microbial biomass (both autotrophic and heterotrophic). Within this context, GPP and ER are functions, among other environmental variables, of the corresponding biomass. In turn, such metabolic fluxes drive, together with the fluxes of carbon uptake, loss, and scouring, the temporal evolution of microbial biomass. Even though the presented case study lacks direct observation on biomass, using biomass as latent variables allowed reproducing fairly well the annual variability of stream metabolism with few parameters, as highlighted by the comparison between our estimates and those obtained with the standard single-station model (Figs. 5, 6).

Studying reaches within the Ybbs River network has shown that, among the variety of different models tested (*see* "Methods" section in Supporting Information), density-dependent biomass growth (i.e., photosynthesis in Eq. 3a, uptake in Eq. 4a, and respiration in Eqs. 5a, 5b) coupled with a linear loss term, explained the observed patterns of streamwater DO concentration reasonably well (Table 4). This suggests that resource competition and acclimation of mature biofilms play a crucial role for ecosystem metabolism. Moreover, the selected model assumes that specific heterotrophic uptake is modulated by DOC concentration (*see* Eq. 4a) and respiration is simply proportional to biomass. Such a model formulation implies that pulses of DOC, related to increases in discharge, for instance, rapidly promote a faster carbon uptake and thus an increase in biomass, which induces, in turn, an increase in the respiration rate. The recent field study by Demars (2019) reports a similar feature.

In all stream reaches, the product between the maximum heterotrophic uptake rate and the density dependence parameter was larger than the autotrophic counterpart ($\mu_{U,20}K_{D_H} > \mu_{P,20}K_{D_A}$, Table 4). This implies that for the same external conditions and reference biomass, heterotrophs grew faster than autotrophs. The interplay between the simulated biomass (B_A, B_H) and the value of the environmental constrains (T, p, Q, PAR) at time t discriminates between an instantaneous carbon sink (NEP(t) > 0) and source (NEP(t) < 0). Moreover, estimating parameters on the basis of a DO time-series with multiple flood events allowed us to isolate, in all the reaches, the effect of peak-flow events on the simulated biomass and, in turn, on metabolic rates (Table 4). The estimation of the parameters governing the loss via scouring is generally challenging because the causes of the damping of the DO signal during a flood event are multiple. They can range from the pure dilution to the increase in the reaeration flux, from the bottom shear stress causing biomass sloughing, to the downturn of biological processes induced by a likewise decrease of other variables such as temperature and/or light, which generally decline during storms. The resulting scouring in study reaches 1, 2, and 3 has a threshold dynamics, with large events activated only during peak discharges (high μ_S and τ_0, Table 4), while site 4 experienced a more continuous removal (low μ_S and τ_0).

By comparing outputs from the single-station approach with those from our model (Figs. 5c, 6c), we have shown that both the temporal dynamics and the magnitude of the simulated fluxes are in approximate agreement. During baseflow and for the same estimate of the reaeration rate, the single-station model could provide a more accurate computation of the GPP and ER for a particular day. Indeed, such a model has 2 free parameters (GPP_d and ER_d, Eq. 9) for each day, and thus can potentially follow DO fluctuations more closely. Conversely, GPP and ER estimated by the proposed model for any particular day depend on the underlying interdaily dynamics of biomass, which is controlled by 11 parameters for the 486 d

simulation period in this case study. From an information content point of view, the single-station model has $2 \times 486 = 972$ free parameters in this application. Therefore, accounting for the underlying dynamics of microbial biomass and integrating information regarding environmental variables (i.e., discharge, temperature, and light) enables a remarkable reduction in model complexity while obtaining comparable estimates of metabolic metrics when sufficiently long time series are considered.

On the other hand, during peak-flow conditions or days with rapidly changing discharge, the estimates of metabolic processes provided by the proposed model could potentially be more reliable than those obtained using the single-station approach. Indeed, estimates of the reaeration rate during high flows are more uncertain because they are extrapolated from field experiments (or from empirical laws based on such experiments, *see*, e.g., Raymond et al. 2012) usually performed under low/mid-flow conditions. Using the single-station model, an error in the reaeration rate directly translates into an error in the estimated GPP and ER for that particular day. Reaeration rates could alternatively be estimated through inverse modeling (Appling et al. 2018*a*). However, during rapidly changing flow conditions, the assumption of stationarity (i.e., equal input and output DO concentration for the focus reach) used to derive Eq. 9 could be problematic. For any specific day instead, metabolism estimates in our approach depend on the microbial biomass and rate parameters estimated using the whole simulation period, and not on the actual reaeration rate. Obviously, errors in the estimation of the reaeration process affect the estimation procedure; however, periods with high flow represent a small fraction of the hydrologic regime and therefore the bulk of the parameter estimation is performed under mid-/low-flow conditions where reaeration estimates and oxygen balance are more reliable.

Using the single-station model, one can estimate GPP and ER only when DO data are available. To extrapolate such estimates to periods with missing data, one needs further assumptions. An approach typically followed is to perform a statistical regression relating daily metabolic fluxes to other environmental variables available throughout the analyzed period (*see*, e.g., Bernhardt et al. 2018). On the other hand, the proposed model offers a straightforward way to extrapolate results to periods when measurements of DO are unavailable, but those of the environmental variables are. Indeed, the model estimates the expected dynamics of DO, and thus the ensuing GPP and ER, given the estimated parameters controlling the underlying temporal dynamics of biomass. The approach is therefore particularly suitable for the calculation of cumulative GPP and ER from high-frequency DO measurements (Table 5), which often contain, even in the best experimental setup, no-data periods.

The proposed model and the single-station method should not be seen as alternatives, but rather as complementary approaches. The model developed here is very data demanding as it needs at least a year-long time series of DO and ancillary variables like light, water temperature, and discharge. Whereas the single-station model can work, in its simplest formulation, with just a single day of DO observation. It is advisable to apply both tools in parallel, as done in this article, to compare and assess model results. An asset of the proposed model is that it provides a link between environmental variables and ecosystem processes and it thus suitable to understand long-term (e.g., seasonal) ecosystem functioning and to possibly predict how changes in environmental variables could impact ecosystem dynamics. For example, it could be possible to estimate the effects of changes in streamwater temperature (e.g., due to climate change or river management), light conditions (e.g., due to riparian clearing), or of the hydrologic regime, characterized for instance by fewer but larger streamflow events—a future evolution predicted by some climatic models. We thus believe that efforts in this direction are crucial to advance our understanding of the response of stream ecosystems to global changes.

Our proposed framework is not exempt from limitations. As stated up front, this model focuses on temporal changes in microbial biomass to explain the variability of metabolic rates that is not explained by changes in light, temperature, and resources; and therefore neglects other possible factors potentially affecting the specific (per unit biomass) metabolic rates. One such a factor could be microbial community composition shifting at the inter- and/or intra-annual timescales. A multiannual time series of observations could allow investigating the former by estimating model parameters separately for each year and analyze if long-term trend are detectable. Community composition shifting within the yearly cycle instead cannot be straightforwardly accounted for in the current model formulation. To that end, one could think of introducing functional forms describing the temporal evolution of some critical parameters or, alternatively, explicitly modeling different microbial functional groups and their interactions. Even in the absence of community composition shifts, it is possible that the intrinsic rates μ and the parameters defining limitation factors are nonstationary in time. In all cases, the net result is the emergence of different metabolic fluxes for the same values of biomass and environmental conditions. In the current model formulation, however, this feature is not permitted and it would likely be reproduced as a biomass variation. Besides the particular problem at hand, the quantification of the variability of metabolic fluxes under the same conditions is a relevant problem for advancing the understanding of stream ecosystem functioning, and one that could likely be addressed via controlled flume experiments. Our results, as well as evidence from direct field observations (*see*, e.g., Uehlinger et al. 1996) point to more than a 10-fold variation in biomass over a yearly cycle. If the variability discussed above were of the same order of magnitude, the application of this framework could be problematic. The same

rationale suggests that stream reaches where low biomass variability is expected (e.g., those with a stable hydrological and thermal regimes) are not particularly suitable to be investigated through the proposed framework in its current formulation.

As illustrated in the "Parameter estimation" section and in Appendix B, whenever biomass is close to equilibrium (Eqs. 11a, 11b), the rate parameters μ and the density dependencies K_D are correlated and equifinal in terms of reproducing the DO signal. This implies that, from measurements of streamwater DO concentration only, it is difficult to infer the actual value of biomass and the rates controlling the carbon fluxes independently. Using longer time series for parameter estimation with longer periods when biomass is far from equilibrium (e.g., scouring events) could allow overcoming such limitation. Moreover, any independent information on biomass or rates could enhance the estimation. Indeed, in this study, we set K_D to realistic values and estimated the rate parameters. As detailed in Appendix B, we stress that, as long as one is not interested in inferring the actual biomass value, the estimation of metabolic processes and carbon fluxes is not impaired by the equifinality issue or by uncertainties in the estimation of K_D values, because such fluxes always depend on the product between biomass and the corresponding rates. Such independent information on biomass or rates could be included in the form of informative prior parameter distributions. Alternatively, if high frequency biomass data (e.g., benthic samples of AFDM and Chl *a*) were available, one could think of estimating parameters including both DO and biomass in the likelihood formulation.

Model formulation enables the estimation of critical carbon fluxes (Fig. 7). Particularly, we have shown how ER can be separated into its autotrophic and heterotrophic components. The estimated fraction of cumulative GPP respired by photoautotrophs (i.e., R_A/GPP) was 0.25 and 0.35 for streams 1 and 2, respectively. These ratios are comparable with the findings of Hall and Beaulieu (2013) who estimated the proportion of primary production respired by autotrophs and closely associated heterotrophs at 44%. We argue, as explained below, that our estimate is closer to the autotrophic physiological values and thus on average lower than 0.44 (*see*, e.g., Graham et al. 1985; Geider and Osborne 1989). Indeed, in our approach, R_A includes only the autotrophic respiration and not the heterotrophic respiration of photosynthetically produced DOC, which is accounted for when applying the 0.9 quantile regression of ER vs. GPP proposed by Hall and Beaulieu (2013). However, we do acknowledge that our partitioning of the modeled carbon fluxes contains caveats and care should be taken therefore when interpreting these outputs. In particular, it is not trivial to separate ER into its autotrophic and heterotrophic components as highlighted by the model outcome from reaches 3 and 4. In the case of reach 3, we argue that such limitations arise because ER overwhelmed photosynthesis (Figs. 6c, 7). Therefore, the autotrophic respiration, which is a constrained fraction of GPP (Del Giorgio and Williams 2005; Hall and Beaulieu 2013), is almost negligible compared to total ER. As a result, variations of parameters controlling R_A have almost no effect on improving the fitting of the time series of streamwater DO concentration, thus the emergent problem of identifiability. The model estimated an R_A close to zero also for reach 4, and this is very likely an underestimation. In this case, the origin of the issue might be related to the resemblance of the predicted seasonal dynamics of the autotrophic and heterotrophic biomass. Indeed, the model ability to separate these two components relies on the fact that their dynamics are driven by different environmental variables (i.e., light and temperature for B_A, temperature and DOC for B_H). However, light and temperature could be highly correlated at seasonal time scales, especially for shallow streams with limited canopy cover, thus producing highly correlated B_A and B_H. In such scenario, the effect of R_A and R_H on the total respiration is almost interchangeable and therefore difficult to resolve.

Our attempt to partition the carbon fluxes highlights the relevance of potential carbon losses other than respiration. For autotrophs, we argue that, besides death and detachment, this flux includes the exudation of photosynthetic carbon, a major loss term in phototrophic biofilms. This is in agreement with empirical observations on the relevance of algal exudates for the carbon cycling within phototrophic biofilms (Haack and McFeters 1982). In the case of heterotrophs, causes of loss other than death may be attributable to grazing by ciliates and other meiofauna that can be highly abundant and diverse in these biofilms (Bengtsson et al. 2018; Weitere et al. 2018). The model estimation of the shear-induced loss of autotrophic biomass may be promising as this may constitute a potentially important source of labile particulate organic carbon (POC) to downstream ER.

It is worth stressing that, as the model is calibrated on oxygen data, carbon fluxes and the related biomass dynamics depend of the photosynthetic and respiratory quotients (RQ) (Eq. 1d) that convert carbon fluxes to oxygen ones. To assess the sensitivity to these parameters, we re-estimated parameters assuming carbon to oxygen RQ (*see* Bott 2011) equal to 0.8 and 1.2 (mol C/mol O_2) (instead of 1) for site 2, as a test case (Supporting Information Figs. S15, S16). In all three cases (RQ = 0.8, 1, 1.2, i.e., $\gamma_A = \gamma_H = 32/(12 \cdot RQ)$), parameters converged to a region such that DO data are well reproduced; and thus they exhibit very similar metabolic fluxes in terms of oxygen (Supporting Information Fig. S15). This implies that for RQ equal to 0.8 (1.2), the corresponding respiration carbon flux is lower (larger) (Supporting Information Fig. S16). However, other carbon fluxes, in particular the loss term, readjust so that all three cases show almost the same biomass temporal pattern (Supporting Information Fig. S15). This result suggests that, in order to reproduce this particular DO time-series, the annual trajectory of biomass is well constrained. Although this test does not represent a comprehensive sensitivity analysis, it suggests that results are not

particularly sensitive to the value assumed for the γ parameters. A possible development worth exploring is the estimation of such parameters jointly with all the others.

Model performance could be possibly increased if nutrients measurements are added to the library of external forcings. This would be a further control on biomass, which would be instrumental for modeling for instance the effect of snowmelt (see, e.g., the peak productivity observed in reach 1 during April 2014, Fig. 5 and DO simulation in "Results" section in Supporting Information), but also of other seasonal effects where temperature and PAR were weak predictors. Such an addition could also allow the overcoming of the above-mentioned limitations of the structural model. An alternative could be to couple an explicit flow routing scheme, enabling the direct estimation of Q_L and thus to consider the groundwater inflow (especially for low order reaches) and/or the snowmelt impact on biomass productivity (e.g., linking such flow to nutrients concentration similarly to what done for DOC concentration). In this case study, we have linked DOC concentration to discharge thus implicitly assuming that temporal variability of DOC is mainly driven by allochthonous inputs. While this assumption could be a reasonable approximation for the case at hand, as detailed in a previous study (Fasching et al. 2016), it may be unsuitable in cases where autochthonous carbon production could significantly contribute to the temporal variability of resources. From a modeling standpoint, this process can be included by accounting for a flux of carbon from the autotrophic to the heterotrophic mass balance, thus effectively coupling the temporal evolution of the autotrophic and heterotrophic biomass.

Another area where improvements are likely possible regards the probabilistic description of the error term. In this first application, we resorted to a simple formulation where all sources of error are encapsulated into a single, additive, IID, Gaussian term. However, it could be possible to formulate more complex structures where different error sources (e.g., process, measurement, estimation of reaeration, etc.) are identified, in line with recent advances in metabolism estimation with open-water methods (Appling et al. 2018*a*). Moreover, the estimation of parameters could benefit from the inclusion of more literature knowledge and physiological constraints via the use of informative prior distributions of parameters (e.g., for the carbon use efficiency [CUE], the photosynthetic and RQ, and the autotrophic respiration fraction, Hall and Beaulieu 2013).

In this study, we presented a novel modeling framework for stream ecosystem metabolism and associated carbon fluxes, and discussed its limitations. We shed light on reach-scale drivers and controls of stream metabolism and moved a step toward a more complete description of ecosystem carbon routing by explicitly modeling critical biological processes. We perceive this research as a basic building block for the development of an integrated, spatially explicit, network-scale model. Indeed, a primary driver of metabolic rates and size of carbon stocks (effectively synthesized in the stream metabolism concept) is the ecosystem size and position along the stream network. The river continuum concept encapsulates this notion, describing how the biological processes and communities are regulated by changes in the physical constraints, from headwaters to the river mouth (Vannote et al. 1980). From this and other conceptual frameworks (Ward and Stanford 1983; Junk et al. 1989; Thorp and Delong 1994; Tockner et al. 2000), it emerges that lateral and vertical fluxes must be investigated at the river network scale. The following step that we deem within reach is the development of a model at the network scale that accounts for the spatial interactions among reaches including geomorphological heterogeneities, external organic carbon supplies, and both hydrological and thermal stochasticity, in the view of the meta-ecosystem theory (Loreau et al. 2003), for instance. Further developments could focus on explicitly simulating DOC and POC stocks (*see* Fig. 1). To that end, other carbon fluxes (e.g., photodegradation, lysis) should be considered. In our view, such a framework is the next step forward to better understand the metabolism of river networks.

APPENDIX A

The final equations for the selected model in the Ybbs case study read:

$$\frac{dB_A}{dt} = (\mu_{P,20} f_L - \mu_{R,A,20}) f_T B_A \left(1 - \frac{B_A}{K_{D,A}}\right) - \mu_{L,A} B_A - \mu_S f_S B_A \quad (10a)$$

$$\frac{dB_H}{dt} = (\mu_{U,20} f_{DOC} - \mu_{R,H,20}) f_T B_H \left(1 - \frac{B_H}{K_{D,H}}\right) - \mu_{L,H} B_H - \mu_S f_S B_H \quad (10b)$$

$$\frac{d\mathrm{DO}}{dt} = Q_{up}[\mathrm{DO}] - Q[\mathrm{DO}] + (\gamma_P \mu_{P,20} f_L - \gamma_R \mu_{R,A,20}) f_T B_A \left(1 - \frac{B_A}{K_{D,A}}\right) - \gamma_H \mu_{R,H,20} f_T B_H \left(1 - \frac{B_H}{K_{D,H}}\right) + K_{DO}([\mathrm{DO}]_{sat} - [\mathrm{DO}]) V \quad (10c)$$

To set biologically meaningful parameter ranges for the prior distribution, we focus on the equilibrium biomass, that is, the non-null equilibrium value such variable would attain for constant external forcings:

$$\bar{B}_A = \left(1 - \frac{\mu_{L,A} + \mu_S f_S}{\mu_{P,20} f_{T,L} - \mu_{R,A,20} f_T}\right) K_{D,A} \quad (11a)$$

$$\bar{B}_H = \left(1 - \frac{\mu_{L,H} + \mu_S f_S}{\mu_{U,20} f_{T,DOC} - \mu_{R,H,20} f_T}\right) K_{D,H} \quad (11b)$$

where the notation $\bar{B}$ refers to biomass at equilibrium conditions. In particular, for the most favorable growth conditions (i.e., maximum light, temperature and DOC, and no scouring), a non-negative equilibrium must exist ($\bar{B} \geq 0$). Moreover,

$\bar{B} \le K_D$ to ensure non-negative carbon fixation and respiration rates. It follows that the terms between parentheses in Eqs. 11a, 11b have to be bounded in [0, 1]. The following constraints are therefore derived:

$$0 \le \frac{\mu_{R,A,20}}{\mu_{P,20} f_{L,\max}} \le 1 \tag{12a}$$

$$0 \le \frac{\mu_{R,H,20}}{\mu_{U,20} f_{\mathrm{DOC},\max}} \le 1 \tag{12b}$$

$$0 \le \frac{\mu_{L,A}}{\left(\mu_{P,20} f_{L,\max} - \mu_{R,A,20}\right) f_{T,\max}} \le 1 \tag{12c}$$

$$0 \le \frac{\mu_{L,H}}{\left(\mu_{U,20} f_{\mathrm{DOC},\max} - \mu_{R,H,20}\right) f_{T,\max}} \le 1 \tag{12d}$$

where the subscript *max* refers to the function computed for the maximum value of the environmental variable. Equations 12a, 12b imply the non-negativity of the growth rate at the most favorable conditions.

Introducing the definition of CUE, that is, the ratio of growth over carbon uptake or fixation, a narrower range can be deduced for Eqs. 12a, 12b.

$$\mathrm{CUE_A}(t) = \frac{P(t) - R_\mathrm{A}(t)}{P(t)} = 1 - \frac{\mu_{R,A,20}}{\mu_{P,20} f_L(t)} \le 1 \tag{13a}$$

$$\mathrm{CUE_H}(t) = \frac{U(t) - R_\mathrm{H}(t)}{U(t)} = 1 - \frac{\mu_{R,H,20}}{\mu_{U,20} f_{\mathrm{DOC}}(t)} \le 1 \tag{13b}$$

According to Eqs. 13a, 13b, CUE $\in$ [0, 1] and CUE is maximum whenever $f_L \to f_{L,\max}$ and $f_{\mathrm{DOC}} \to f_{\mathrm{DOC},\max}$. Following Hall and Beaulieu (2013), we assume that the maximum autotrophic CUE has to be greater than 40%, that is, at least 40% of the fixed carbon goes into biomass and is not used as energy source for other biological processes, an upper bound of 0.6 can be imposed for the inequality (12a). The same rationale is less straightforward for the heterotrophic processes given the different anabolic pattern and this is why a more conservative minimum CUE of 10% at the most favorable conditions has been imposed (Del Giorgio and Cole 1998), that is, an upper bound of 0.9 can be set for Eq. 12b. Finally, for the last two constraints, 12c and 12d, it is reasonable to assume that loss rate at best external conditions, is lower than the growth rate. Preliminary tests have shown that the Markov chains never reach values greater than 50%, which has therefore been used as upper bound. A nonzero lower bound of 10^{-3} has been set for numerical reasons.

APPENDIX B

To investigate possible parameter equifinality, we first approximate the model by assuming that both biomass variables (B_A and B_H) are in equilibrium with the daily averaged forgings (i.e., separation of fast and slow dynamics). Under such hypothesis, we can substitute the expressions for the equilibrium biomass (Eqs. 11a, 11b) into the measurement model (Eq. 1d), thus obtaining:

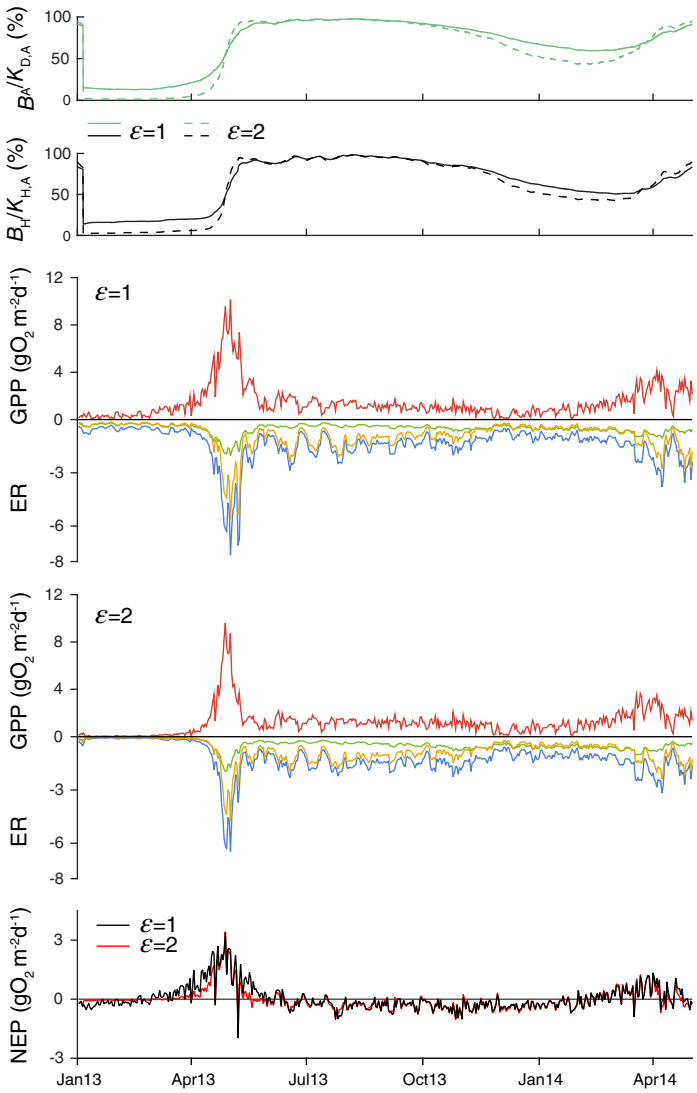

Fig. B1 Comparison between model results for site 2 obtained using the estimated parameters reported in Table 4 (case ϵ = 1) and those obtained by halving the density dependencies (K_D) and doubling the specific metabolic rates (μ), (case ϵ = 2).

$$\frac{d\mathrm{DO}(t)}{dt} = \bar{f}_T\left(\gamma_P K_{D,A}\mu_{P,20}\bar{f}_L - \gamma_A K_{D,A}\mu_{R,A,20}\right) \times \left(\frac{\mu_{L,A}+\mu_S\bar{f}_S}{\mu_{P,20}\bar{f}_{T,L}-\mu_{R,A,20}\bar{f}_T}\right)\left(1-\frac{\mu_{L,A}+\mu_S\bar{f}_S}{\mu_{P,20}\bar{f}_{T,L}-\mu_{R,A,20}\bar{f}_T}\right) + -\bar{f}_T\gamma_H K_{D,H}\mu_{R,H,20} \times \left(\frac{\mu_{L,H}+\mu_S\bar{f}_S}{\mu_{U,20}\bar{f}_{T,\mathrm{DOC}}-\mu_{R,H,20}\bar{f}_T}\right)\left(1-\frac{\mu_{L,H}+\mu_S\bar{f}_S}{\mu_{U,20}\bar{f}_{T,\mathrm{DOC}}-\mu_{R,H,20}\bar{f}_T}\right) + + K_{\mathrm{DO}}(t)(\mathrm{DO}_{\mathrm{sat}}(t)-\mathrm{DO}(t)) \quad (14)$$

where the symbol $\bar{f}$ refers to the corresponding functions computed using daily averaged environmental variables. Let us now consider different model simulations with parameters $[K_{D,A};\ \mu_{P,20};\ \mu_{R,A,20};\ \mu_{L,A};\ \mu_S] = [x_1/\epsilon; x_2\epsilon; x_3\epsilon; x_4\epsilon; x_5\epsilon]$ obtained changing $\epsilon > 0$ for a fix, yet arbitrary, $[x_1, \ldots, x_5]$. We limit the analysis to autotrophic parameters for brevity, but the same reasoning applies to heterotrophic ones. From Eq. 14, it is straightforward to see that different values of ϵ produce identical trajectories for DO—the only observed variable. Therefore, density-dependent parameters and ecosystem rates are equifinal. This holds exactly under the equilibrium assumption stated above. While such assumption is reasonable for the processes of photosynthesis, carbon uptake, respiration, and loss, which have a time scale shorter than the seasonal fluctuations of the light and temperature regime; variations of discharge (and the ensuing bottom shear stress and scouring process) occur at a much faster time scale and can thus temporarily push biomass out of equilibrium conditions. However, such events seldom occur in our case study (*see* "Results" section) and therefore, for the majority of the parameter estimation period, density-dependent and ecosystem-rate parameters are approximately equifinal and this leads to the correlation observed in the preliminary tests.

To further illustrate this equifinality, we perform an experiment using site 2 and modifying the estimated parameters (Table 4) setting ϵ = 2, that is, halving the density dependencies and doubling all specific metabolic rates for both autotrophs and heterotrophs, while keeping the remaining parameters fixed (Fig. B1). Biomass temporal dynamics result very similar when close to equilibrium, slightly deviate during winter (when productivity is low compared to loss) and after the major scouring event in January 2013 (strong out-of-equilibrium conditions), while producing very similar DO trajectories ($\mathrm{RMSE}_{\mathrm{DO\%}}$ = 1.630%). As detailed above, biological fluxes, and in particular GPP and ER, are not affected by the choice of the density dependence parameters (Fig. B1).

APPENDIX C

Table C1 Mathematical symbols used in the text and their definition.

Symbol	Definition	Unit adopted
State variables		
V	Control volume	m^3
B_A	Autotrophic biomass	g C
B_H	Heterotrophic biomass	g C
DO	Dissolved mass of oxygen	g O_2
Forcing variables		
T	Water temperature	°C
PAR	Photosynthetically active radiation	lx
p	Barometric pressure	atm
Q	Discharge exiting the local node	$m^3\ d^{-1}$
Site geometry and hydraulic variables		
z	Reach water depth	m
A	Reach bed area	m^2
τ	Bottom shear stress	Pa
τ_0	Minimum shear stress needed to activate scouring	Pa
Hydrological fluxes		
Q	Discharge exiting the control volume	$m^3\ d^{-1}$
Q_L	Incoming/outgoing lateral discharge	$m^3\ d^{-1}$
Q_{up}	Incoming discharge from upstream	$m^3\ d^{-1}$
ϕ	DO mass flux exiting the control volume	g $O_2\ d^{-1}$
ϕ_L	Incoming/outgoing lateral DO mass flux	g $O_2\ d^{-1}$
ϕ_{up}	DO mass flux entering the reach from upstream	g $O_2\ d^{-1}$
Bio-physical fluxes		
P	Photosynthetic rate	g C d^{-1}
R_A	Autotrophic respiration rate	g C d^{-1}
L_A	Autotrophic loss rate	g C d^{-1}
S_A	Scouring rate of autotrophic biomass	g C d^{-1}
U	Uptake rate	g C d^{-1}
R_H	Heterotrophic respiration rate	g C d^{-1}
L_H	Heterotrophic loss rate	g C d^{-1}
S_H	Scouring rate of heterotrophic biomass	g C d^{-1}
R_e	DO reaeration rate	g $O_2\ d^{-1}$
GPP	Gross primary production (daily, per unit area)	g $O_2\ m^{-2}\ d^{-1}$
ER	Ecosystem respiration (daily, per unit area)	g $O_2\ m^{-2}\ d^{-1}$
NEP	Net ecosystem production (daily, per unit area)	g $O_2\ m^{-2}\ d^{-1}$
Bio-physical parameters and rates		
γ_P	Mass of DO photosynthesized per unit mass of C fixed	g O_2 g C^{-1}

(Continues)

Table C1. Continued

Symbol	Definition	Unit adopted
γ_A	Mass of DO respired by B_A per unit mass of C consumed	g O_2 g C^{-1}
γ_H	Mass of DO respired by B_H per unit mass of C consumed	g O_2 g C^{-1}
$\mu_{P,20}$	Maximum specific photosynthetic rate at 20°	d^{-1}
$K_{D,A}$	Autotrophic density dependency	g C
θ_A	Autotrophic temperature dependence parameter	-
K_{PAR}	Light half saturation	lx
$\mu_{U,20}$	Maximum specific uptake rate at 20°	d^{-1}
$K_{D,H}$	Heterotrophic density dependency	g C
θ_H	Heterotrophic temperature dependence parameter	-
$\mu_{R,A,20}$	Maximum specific autotrophic respiration rate at 20°	d^{-1}
$\mu_{R,H,20}$	Maximum specific heterotrophic respiration rate at 20°	d^{-1}
$\mu_{L,A}$	Autotrophic specific loss rate	d^{-1}
$\mu_{L,H}$	Heterotrophic specific loss rate	d^{-1}
μ_S	Specific scouring rate	d^{-1}
K_{DO}	Oxygen mass transfer coefficient	d^{-1}
Others		
a	Reach drainage area	km^2
[DOC]	Local dissolved organic carbon concentration	g C m^{-3}
$[DO]_{sat}$	Local dissolved oxygen saturation concentration	g O_2 m^{-3}
$DO_{\%}$	Simulated dissolved oxygen percentage from saturation	%
$DO_{\%Obs}$	Observed dissolved oxygen percentage from saturation	%
γ_w	Specific weight of water	N m^{-3}
CUE	Carbon use efficiency	g C g C^{-1}

References

Acuña, V., A. Wolf, U. Uehlinger, and K. Tockner. 2008. Temperature dependence of stream benthic respiration in an Alpine river network under global warming. Freshw. Biol. **53**: 2076–2088. doi:10.1111/j.1365-2427.2008.02028.x

Acuña, V., and K. Tockner. 2010. The effects of alterations in temperature and flow regime on organic carbon dynamics in Mediterranean river networks. Glob. Chang. Biol. **16**: 2638–2650. doi:10.1111/j.1365-2486.2010.02170.x

Appling, A. P., R. O. Hall, C. B. Yackulic, and M. Arroita. 2018*a*. Overcoming equifinality: Leveraging long time series for stream metabolism estimation. J. Geophys. Res. Biogeosci. **123**: 624–645. doi:10.1002/2017jg004140

Appling, A. P., and others. 2018*b*. The metabolic regimes of 356 rivers in the United States. Sci. Data **5**. doi:10.1038/sdata.2018.292

Battin, T. J., L. A. Kaplan, S. Findlay, C. S. Hopkinson, E. Marti, A. I. Packman, J. D. Newbold, and F. Sabater. 2008. Biophysical controls on organic carbon fluxes in fluvial networks. Nat. Geosci. **1**: 95–100. doi:10.1038/ngeo101

Battin, T. J., S. Luyssaert, L. A. Kaplan, A. K. Aufdenkampe, A. Richter, and L. J. Tranvik. 2009. The boundless carbon cycle. Nat. Geosci. **2**: 598–600. doi:10.1038/ngeo618

Battin, T. J., K. Besemer, M. M. Bengtsson, A. M. Romani, and A. I. Packmann. 2016. The ecology and biogeochemistry of stream biofilms. Nat. Rev. Microbiol. **14**: 251–263. doi:10.1038/ngeo618

Bellmore, J. R., A. K. Fremier, F. Mejia, and M. Newsom. 2014. The response of stream periphyton to pacific salmon: Using a model to understand the role of environmental context. Freshw. Biol. **59**: 1437–1451. doi:10.1111/fwb.12356

Bengtsson, M. M., K. Wagner, C. Schwab, T. Urich, and T. J. Battin. 2018. Light availability impacts structure and function of phototrophic stream biofilms across domains and trophic levels. Mol. Ecol. **27**: 2913–2925. doi:10.1111/mec.14696

Bernhardt, E. S., and others. 2018. The metabolic regimes of flowing waters. Limnol. Oceanogr. **63**: S99–S118. doi:10.1002/lno.10726

Billen, G., J. Garnier, and P. Hanset. 1994. Modelling phytoplankton development in whole drainage networks: The RIVERSTRAHLER model applied to the seine river system, p. 119–137. *In* J. P. Jesky, C. S. Reynlods, and J. Padisák [eds.], Phytoplankton in turbid environments: Rivers and shallow lakes. Springer. doi:10.1007/978-94-017-2670-2_11

Bott, T., J. Brock, C. Cushing, S. Gregory, D. King, and R. Petersen. 1978. A comparison of methods for measuring primary productivity and community respiration in streams. Hydrobiologia **60**: 3–12. doi:10.1016/b978-012332908-0.50040-1

Bott, T. L. 2011. Chapter 28: Primary productivity and community respiration, p. 663–690. *In* F. R. Hauer and G. Lamberti [eds.], Methods in stream ecology. Academic Press.

Burnham, K. P., and D. R. Anderson. 2003. Model selection and multimodel inference: A practical information-theoretic approach. Springer Science & Business Media.

Burris, J. 1981. Effects of oxygen and inorganic carbon concentrations on the photosynthetic quotients of marine algae. Mar. Biol. **65**: 215–219. doi:10.1007/bf00397114

Carraro, L., M. Toffolon, A. Rinaldo, and E. Bertuzzo. 2019. Sestet: A spatially-explicit stream temperature model based on equilibrium temperature. Hydrol. Process. doi:10.1002/hyp.13591

Ceola, S., E. Bertuzzo, G. Singer, T. J. Battin, A. Montanari, and A. Rinaldo. 2014. Hydrologic controls on basin-scale

distribution of benthic invertebrates. Water Resour. Res. **50**: 2903–2920. doi:10.1002/2013wr015112

Cole, J. J., and others. 2007. Plumbing the global carbon cycle: Integrating inland waters into the terrestrial carbon budget. Ecosystems **10**: 172–185. doi:10.1007/s10021-006-9013-8

Del Giorgio, P. A., and J. J. Cole. 1998. Bacterial growth efficiency in natural aquatic systems. Annu. Rev. Ecol. Syst. **29**: 503–541. doi:10.1146/annurev.ecolsys.29.1.503

Del Giorgio, P. A., and P. L. B. Williams. 2005. The global significance of respiration in aquatic ecosystems: From single cells to the biosphere, p. 267–303. *In* Respiration in aquatic ecosystems. Oxford University Press.

DeLong, J. P., T. C. Hanley, and D. A. Vasseur. 2014. Competition and the density dependence of metabolic rates. J. Anim. Ecol. **83**: 51–58. doi:10.1111/1365-2656.12065

Demars, B. O. 2019. Hydrological pulses and burning of dissolved organic carbon by stream respiration. Limnol. Oceanogr. **64**: 406–421. doi:10.1002/lno.11048

Demars, B. O., J. Thompson, and J. R. Manson. 2015. Stream metabolism and the open diel oxygen method: Principles, practice, and perspectives. Limnol. Oceanogr.: Methods **13**: 356–374. doi:10.1002/lom3.10030

Demars, B. O., G. M. Gíslason, J. S. Ólafsson, J. R. Manson, N. Friberg, J. M. Hood, J. J. Thompson, and T. E. Freitag. 2016. Impact of warming on CO_2 emissions from streams countered by aquatic photosynthesis. Nat. Geosci. **9**: 758–761. doi:10.1038/ngeo2807

Fasching, C., B. Behounek, G. A. Singer, and T. J. Battin. 2014. Microbial degradation of terrigenous dissolved organic matter and potential consequences for carbon cycling in brown-water streams. Sci. Rep. **4**: 4981. doi:10.1038/srep04981

Fasching, C., A. J. Ulseth, J. Schelker, G. Steniczka, and T. J. Battin. 2016. Hydrology controls dissolved organic matter export and composition in an Alpine stream and its hyporheic zone. Limnol. Oceanogr. **61**: 558–571. doi:10.1002/lno.10232

Flipo, N., S. Even, M. Poulin, M. H. Tusseau-Vuillemin, T. Ameziane, and A. Dauta. 2004. Biogeochemical modelling at the river scale: Plankton and periphyton dynamics: Grand Morin case study, France. Ecol. Model. **176**: 333–347. doi:10.1016/j.ecolmodel.2004.01.012

Flipo, N., C. Rabouille, M. Poulin, S. Even, M. H. Tusseau-Vuillemin, and M. Lalande. 2007. Primary production in headwater streams of the Seine basin: The Grand Morin river case study. Sci. Total Environ. **375**: 98–109. doi:10.1016/j.scitotenv.2006.12.015

Geider, R. J., and B. A. Osborne. 1989. Respiration and microalgal growth: A review of the quantitative relationship between dark respiration and growth. New Phytol. **112**: 327–341. doi:10.1111/j.1469-8137.1989.tb00321.x

Gelman, A., and D. B. Rubin. 1992. Inference from iterative simulation using multiple sequences. Stat. Sci. **7**: 457–472. doi:10.1214/ss/1177011136

Grace, M. R., D. P. Giling, S. Hladyz, V. Caron, R. M. Thompson, and R. Mac Nally. 2015. Fast processing of diel oxygen curves: Estimating stream metabolism with BASE (BAyesian Single-station Estimation). Limnol. Oceanogr.: Methods **13**: 103–114. doi:10.1002/lom3.10011

Graham, J. M., J. A. Kranzfelder, and M. T. Auer. 1985. Light and temperature as factors regulating seasonal growth and distribution of *Ulothrix zonata* (Ulvophyceae). J. Phycol. **21**: 228–234. doi:10.1111/j.0022-3646.1985.00228.x

Haack, T. K., and G. A. McFeters. 1982. Nutritional relationships among microorganisms in an epilithic biofilm community. Microb. Ecol. **8**: 115–126. doi:10.1007/bf02010445

Hall, R. O., Jr., and J. J. Beaulieu. 2013. Estimating autotrophic respiration in streams using daily metabolism data. Freshw. Sci. **32**: 507–516. doi:10.1899/12-147.1

Hall, R. O., Jr., C. B. Yackulic, T. A. Kennedy, M. D. Yard, E. J. Rosi-Marshall, N. Voichick, and K. E. Behn. 2015. Turbidity, light, temperature, and hydropeaking control primary productivity in the Colorado River, Grand Canyon. Limnol. Oceanogr. **60**: 512–526. doi:10.1002/lno.10031

Holtgrieve, G. W., D. E. Schindler, T. A. Branch, and Z. T. A'mar. 2010. Simultaneous quantification of aquatic ecosystem metabolism and reaeration using a Bayesian statistical model of oxygen dynamics. Limnol. Oceanogr. **55**: 1047–1063. doi:10.4319/lo.2010.55.3.1047

Hotchkiss, E. R., and R. O. Hall Jr. 2014. High rates of daytime respiration in three streams: Use of $\delta^{18}O_2$ and O_2 to model diel ecosystem metabolism. Limnol. Oceanogr. **59**: 798–810. doi:10.4319/lo.2014.59.3.0798

Jäger, C. G., and D. Borchardt. 2018. Longitudinal patterns and response lengths of algae in riverine ecosystems: A model analysis emphasising benthic-pelagic interactions. J. Theor. Biol. **442**: 66–78. doi:10.1016/j.jtbi.2018.01.009

Jassby, A. D., and T. Platt. 1976. Mathematical formulation of the relationship between photosynthesis and light for phytoplankton. Limnol. Oceanogr. **21**: 540–547. doi:10.4319/lo.1976.21.4.0540

Jørgensen, S. E., and G. Bendoricchio. 2001. Fundamentals of ecological modelling, v. **21**. Elsevier.

Junk, W. J., P. B. Bayley, and R. E. Sparks. 1989. The flood pulse concept in river-floodplain systems. Can. Spec. Publ. Fish. Aquat. Sci. **106**: 110–127. doi:10.1127/lr/11/1999/261

Loreau, M., N. Mouquet, and R. D. Holt. 2003. Meta-ecosystems: A theoretical framework for a spatial ecosystem ecology. Ecol. Lett. **6**: 673–679. doi:10.1046/j.1461-0248.2003.00483.x

McIntire, C. D. 1973. Periphyton dynamics in laboratory streams: A simulation model and its implications. Ecol. Monogr. **43**: 399–420. doi:10.2307/1942348

McIntire, C. D., and H. K. Phinney. 1965. Laboratory studies of periphyton production and community metabolism in lotic environments. Ecol. Monogr. **35**: 237–258. doi:10.2307/1942138

McIntire, C. D., and J. A. Colby. 1978. A hierarchical model of lotic ecosystems. Ecol. Monogr. **48**: 167–190. doi:10.2307/2937298

Naegeli, M. W., and U. Uehlinger. 1997. Contribution of the hyporheic zone to ecosystem metabolism in a prealpine gravel-bed-river. J. N. Am. Benthol. Soc. **16**: 794–804. doi:10.2307/1468172

Odum, H. T. 1956. Primary production in flowing waters. Limnol. Oceanogr. **1**: 102–117. doi:10.4319/lo.1956.1.2.0102

Palmeri, L., A. Barausse, and S. E. Jørgensen. 2013. Ecological processes handbook. CRC Press.

Raymond, P. A., and others. 2012. Scaling the gas transfer velocity and hydraulic geometry in streams and small rivers. Limnol. Oceanogr.: Fluids Environ. **2**: 41–53. doi:10.1215/21573689-1597669

Regnier, P., and others. 2013. Anthropogenic perturbation of the carbon fluxes from land to ocean. Nat. Geosci. **6**: 597–607. doi:10.1038/ngeo1830

Roman, A. M., and S. Sabater. 1999. Effect of primary producers on the heterotrophic metabolism of a stream biofilm. Freshw. Biol. **41**: 729–736. doi:10.1046/j.1365-2427.1999.00413.x

Schelker, J., G. A. Singer, A. J. Ulseth, S. Hengsberger, and T. J. Battin. 2016. CO_2 evasion from a steep, high gradient stream network: Importance of seasonal and diurnal variation in aquatic pCO_2 and gas transfer. Limnol. Oceanogr. **61**: 1826–1838. doi:10.1002/lno.10339

Song, C., and others. 2018. Continental-scale decrease in net primary productivity in streams due to climate warming. Nat. Geosci. **11**: 415. doi:10.1038/s41561-018-0125-5

Tank, J. L., E. J. Rosi-Marshall, N. A. Griffiths, S. A. Entrekin, and M. L. Stephen. 2010. A review of allochthonous organic matter dynamics and metabolism in streams. J. N. Am. Benthol. Soc. **29**: 118–146. doi:10.1899/08-170.1

Ter Braak, C. J., and J. A. Vrugt. 2008. Differential evolution Markov chain with snooker updater and fewer chains. Stat. Comput. **18**: 435–446. doi:10.1007/s11222-008-9104-9

Thorp, J. H., and M. D. Delong. 1994. The riverine productivity model: An heuristic view of carbon sources and organic processing in large river ecosystems. Oikos **70**: 305–308. doi:10.2307/3545642

Tockner, K., F. Malard, and J. Ward. 2000. An extension of the flood pulse concept. Hydrol. Process. **14**: 2861–2883. doi:10.1002/1099-1085(200011/12)14:16/17<2861::AID-HYP124>3.0.CO;2-F

Trimmer, M., J. Grey, C. M. Heppell, A. G. Hildrew, K. Lansdown, H. Stahl, and G. Yvon-Durocher. 2012. River bed carbon and nitrogen cycling: State of play and some new directions. Sci. Total Environ. **434**: 143–158. doi:10.1016/j.scitotenv.2011.10.074

Uehlinger, U., H. Bührer, and P. Reichert. 1996. Periphyton dynamics in a floodprone prealpine river: Evaluation of significant processes by modelling. Freshw. Biol. **36**: 249–263. doi:10.1046/j.1365-2427.1996.00082.x

Uehlinger, U., and M. W. Naegeli. 1998. Ecosystem metabolism, disturbance, and stability in a prealpine gravel bed river. J. N. Am. Benthol. Soc. **17**: 165–178. doi:10.2307/1467960

Ulseth, A. J., E. Bertuzzo, G. A. Singer, J. Schelker, and T. J. Battin. 2018. Climate-induced changes in spring snowmelt impact ecosystem metabolism and carbon fluxes in an alpine stream network. Ecosystems **21**: 373–390. doi:10.1007/s10021-017-0155-7

Van de Bogert, M. C., S. R. Carpenter, J. J. Cole, and M. L. Pace. 2007. Assessing pelagic and benthic metabolism using free water measurements. Limnol. Oceanogr.: Methods **5**: 145–155. doi:10.4319/lom.2007.5.145

Vannote, R. L., G. W. Minshall, K. W. Cummins, J. R. Sedell, and C. E. Cushing. 1980. The river continuum concept. Can. J. Fish. Aquat. Sci. **37**: 130–137. doi:10.1515/ijnsns.2009.10.3.273

Vrugt, J. A., C. Ter Braak, C. Diks, B. A. Robinson, J. M. Hyman, and D. Higdon. 2009. Accelerating Markov Chain Monte Carlo simulation by differential evolution with self-adaptive randomized subspace sampling. Int. J. Nonlin. Sci. Num. Simul. **10**: 273–290.

Ward, J. V., and J. Stanford. 1983. The serial discontinuity concept of lotic ecosystems, p. 29–42. *In* Dynamics of lotic ecosystems. Ann Arbor Science.

Weitere, M., and others. 2018. The food web perspective on aquatic biofilms. Ecol. Monogr. **88**: 543–559. doi:10.1002/ecm.1315

Wilcock, R. J., J. W. Nagels, G. B. McBride, K. J. Collier, B. T. Wilson, and B. A. Huser. 1998. Characterisation of lowland streams using a single-station diurnal curve analysis model with continuous monitoring data for dissolved oxygen and temperature. N. Z. J. Mar. Freshw. Res. **32**: 67–79. doi:10.1080/00288330.1998.9516806

Wootton, J. T., M. S. Parker, and M. E. Power. 1996. Effects of disturbance on river food webs. Science **273**: 1558–1561. doi:10.1126/science.273.5281.1558

Acknowledgments

We are grateful to Amber Ulseth for sharing data of the study streams in the Ybbs River Network. Financial support was provided by the Swiss Science Foundation (METALP, grant 200021_163015) to T.J.B. and P.L.S. and by the University of Venice Ca′ Foscari (Project IRIDE) to E.B.

Conflict of Interest

None declared.

Submitted 06 October 2018
Revised 19 March 2019
Accepted 16 November 2019

Associate editor: Ryan Sponseller